The Cryosphere Discuss., doi:10.5194/tc-2016-219, 2016
Manuscript under review for journal The Cryosphere
Published: 30 September 2016

The Cryosphere Discussions
Open Access

Characterizing sudden changes in Arctic sea ice drift and deformation on synoptic timescales

Jennifer V. Lukovich[1], Cathleen A. Geiger[2], David G. Barber[1]

[1]Centre for Earth Observation Science, University of Manitoba, Winnipeg, R3T 2N2, CANADA
[2]College of Earth, Ocean, and Environment: Geography, University of Delaware, Delaware, 19716, USA

Correspondence to: Jennifer V. Lukovich (Jennifer.Lukovich@umanitoba.ca)

Abstract. In this study, we develop a framework for the assessment of sudden changes in sea ice drift and associated deformation processes in response to atmospheric forcing and ice-coastal interactions, based on analysis of ice buoy triplet centroids and areas. Examined in particular is the spatiotemporal evolution in sea ice floes that are tracked with GPS beacons deployed in triplets in the southern Beaufort Sea at varying distances from the coastline in fall, 2009 – triplets A to D, with A (D) located closest to (furthest from) the coastline. This study illustrates the use of shock-response diagnostics to evaluate eight identified sudden changes or shock events on daily timescales. Results from this analysis show that shock events in the southern Beaufort Sea occur in at least one of two forms: (1) during a reversal in winds, or (2) sustained north/easterly winds, with response mechanisms governed by ice conditions and interactions with the coastline. Demonstrated also is the emergence of a shear-shock event (SSE) that results in reduced ice concentrations for triplets B, C, and D, one, three and five days following the SSE, respectively and loss of synchronicity in ice-atmosphere interactions. The tools developed in this study provide a unique characterization of sea ice dynamical processes in the southern Beaufort Sea, with implications for quantifying "shock-response" systems relevant for ice hazard assessments and forecasting applications required by oil and gas, marine transportation, and indigenous use of near shore Arctic areas.

1 Introduction

When the ice cover on polar seas changes suddenly, navigation channels are altered as a result of ice-ice and ice-coastline momentum and energy flux exchanges (e.g., The Polar Group, 1980; Hwang, 2005; McPhee, 2012), air-sea heat exchanges increase (e.g., Carmack et al., 2015), and newly opened leads vent high moisture into the atmosphere as a strong mass exchange process (Bourassa et al., 2013). Understanding how these changes develop and relate to the orientation of a coastline is essential when diagnosing response patterns. For clarity, sudden change in this study refers to changes in the ice drift path relative to storm tracks, which have typical duration on the order of days and recurrence rates on the order of several days to weeks.

Arctic air-ice-sea interactions on synoptic timescales (several days to weeks) are governed by a force balance consisting of three interactive components: i) sea ice motion, ii) a confining coastline, and iii) atmospheric forcing. Previous studies have examined sea ice drift and deformation response to atmospheric forcing and coastline geometry on varying timescales (Overland et al., 1995; Richter-Menge et al., 2002; Geiger and Perovich, 2008; Hutchings et al., 2011). In an assessment of springtime sea ice drift in a region to the west of the Antarctic Peninsula, Geiger and Perovich (2008) identified low-frequency motion in response to atmospheric forcing and coastal geometry associated with regional-scale transport, and higher-frequency near-inertial oscillatory motion associated with mixing. On regional and synoptic scales, Richter-Menge et al. (2002) also distinguish between translational and differential motion associated with shear zones and discontinuities in the ice drift characteristics in the southern Beaufort Sea.

The role of forcing (wind stress) and coastline geometry in establishing coherence in lead patterns/fractures in the ice cover captured by sea ice deformation has also been explored in past studies (Overland et al., 1995; Hutchings et al., 2005, 2011). Overland et al. (1995) demonstrated that in the Beaufort Sea for spatial scales: i) exceeding 100 km the sea ice cover moves as an aggregate; ii) less than 100 km the ice cover moves as an aggregate or discrete entity based on whether an elliptic (homogeneous) or hyperbolic (discrete) regime is established relative to the coastline (ice-coast interactions); and iii) on the order of 1 km the ice cover is characterized by floe (ice-ice) interactions. Through analysis of a nested beacon configuration and array with spatial scales ranging from 10 km to 140 km as part of the late winter (April) 2007 Sea Ice Experiment: Dynamic Nature of the Arctic (SEDNA) campaign in the Beaufort Sea, Hutchings et al. (2011) demonstrated coherence between 140 km and 20km divergence arrays for time periods of up to 16 days in March. Over shorter (sub-synoptic) timescales from May 2007 onward, nested buoy arrays captured the loss of connectivity in the sea ice cover associated with the winter-to-summer transition during a substantial ice-loss year (Stroeve et al., 2008).

In this study, we extend these analyses to quantify changes in the ice cover and in particular to explore sea ice drift and deformation in response to on-, off-, and along-shore winds based on distance from the coastline. For simplicity and for the synoptic timescales considered in this study, we ignore lower-frequency ocean current fluctuations. We also ignore higher-frequency fluctuations associated with inertial oscillations, which are explored in a companion paper (Geiger and Lukovich, in preparation). We instead focus here on the spatiotemporal synoptic changes in sea ice drift and deformation that are directly related to storm tracks while they are developing and migrating through a local region, using a novel observational and analytical approach based on a three-particle dispersion analysis and evolution of beacons deployed in a triangular configuration as triplets

Central to an understanding of sea ice drift and deformation in response to atmospheric forcing and ice-coastline interactions is the development of diagnostics and in the case of drifting buoys, a Lagrangian framework to quantify spatiotemporal changes in the ice cover. Previous studies have used Lagrangian dispersion and ice beacon trajectories to quantify sea ice drift and deformation in the Arctic (Colony and Thorndike, 1984, 1985; Rampal, 2008, 2009a,b; Lukovich et al., 2011, 2014, 2015). Single-particle (absolute) dispersion provides a signature of large-scale circulation and captures linear time-dependence in fluctuating velocity variance characteristic of turbulent diffusion theory (Taylor, 1921; Rampal et al., 2009); i.e., departures in ice fluctuating velocity statistics from turbulent diffusion are attributed to intermittency associated with sea ice deformation and internal ice stress (Rampal et al., 2009).

A two-particle (relative) dispersion analysis monitors sea ice deformation. Through evaluation of buoy pair separations as a proxy of strain-rate (divergence, convergence, and strain) components combined, two-particle dispersion demonstrates heterogeneity and intermittency in the sea ice deformation field associated with space/time coupling inherent in fracturing of the sea ice cover as described by sea ice mechanics (Rampal et al., 2008; Weiss, 2013). Rampal et al. (2008) noted that a triplet or multiple-particle analysis is in addition necessary to illustrate the deformation and related small-scale kinematic features that develop in sea ice.

Three -particle dispersion and triplet areas in particular, such as are explored in this study, enable a distinction between the individual strain-rate tensor components of divergence, convergence, and shear. Specifically, sea ice divergence depicts open water formation and accompanying processes such as new ice growth, brine rejection to the ocean, and heat and moisture exchange; ice convergence depicts ridge and keel formation thus contributing to ice thickness (Stern and Lindsay, 2009; Kwok and Cunningham, 2012), with implications for ice hazard detection, oil spill and contaminant transport and shipping route assessments. Triplet areas also provide a signature of what is referred to by Thorndike (1986) as "nondivergent diffusive mixing" due to compressibility in the ice cover.

Early studies of oceanic circulation have used multiple particles to monitor small-scale deformation and mixing as opposed to larger-scale stirring mechanisms captured by single-particle dispersion analyses. Ice beacon triplet arrays have also been used to monitor sea ice deformation off the Canadian east coast and in Antarctica (Prinsenberg et al., 1997; Heil et al., 2002; 2008; 2009; 2011). Studies of correspondence between ice stress, convergence and atmospheric forcing off the southern coast of Labrador in March, 1996 showed little change in convergence within an already compact ice cover, in addition to an increase in stress with winds and decrease in stress with temperature as the icepack loses its ability to transmit pressure (Prinsenberg et al., 1997). These results are consistent with studies of derived ice motion fields using synthetic aperture radar data showing sea ice deformation and production 1.5 times higher in the seasonal than in the perennial ice zone throughout the Arctic in late fall and winter due to differences in ice strength and thickness (Kwok, 2006).

Application of Lagrangian dispersion (single- and two-particle) in the Beaufort Sea region in past studies showed that single-particle dispersion captures the existence of two distinct dynamical regimes characterized by distinctive scaling laws; t^2 scaling in the zonal direction characteristic of advection, and $t^{5/4}$ scaling in the meridional direction characteristic of quasi-geostrophic 2D turbulence (Lukovich et al., 2011). Two-particle dispersion studies in this region, based on an assessment of loop and meander reversal events, demonstrated enhanced meridional separation indicative of ice-ice and ice-coast interactions and increased connectivity in the ice cover in winter relative to spring (Lukovich et al., 2014).

In the present study we build upon these previous analyses to provide, using three-particle dispersion analyses, a prescription for changes in sea ice drift trajectories and deformation in response to atmospheric forcing and coastal interactions for varying distances from the coastline. In particular, we seek to address the following research questions:

The Cryosphere Discuss., doi:10.5194/tc-2016-219, 2016
Manuscript under review for journal The Cryosphere
Published: 30 September 2016

i) What is the correspondence between sudden changes in sea ice drift trajectories, atmospheric forcing, and distance relative to the coastline on daily and more generally synoptic timescales? [How can individual sea ice drift events be characterized?]

ii) How are sudden changes manifested in deformation characteristics? How do these characteristics vary daily based on orientation (near shore, offshore, and along shore) and distance relative to the coast?

The goal of this paper is to develop a framework for understanding sudden changes in ice drift trajectories in the Beaufort Sea on daily and synoptic timescales using triplet centroids and areas to quantify drift and deformation, respectively, with the potential for application to an assessment of dynamical regimes in other regions of the Arctic.

The paper proceeds as follows. Data used to identify sudden changes in sea ice drift are described in Section 2. In Section 3, methods based on three-particle dispersion and the triplet area approach, are presented. Results associated with each of the two objectives are provided in Section 4, followed by discussions of results in the context of sudden changes in Section 5, and in Section 6 conclusions in addition to a short description of future work.

2 Data

Sea ice position data were obtained from an array of ten ice beacons and one ice mass balance buoy launched from the CCGS *Amundsen* in the marginal ice zone of the southern Beaufort Sea in September, 2009 (Figure 1 and Table I). From this array, four triangular configurations were selected, hereinafter referred to as triplets A to D, to monitor divergence and convergence of sea ice, with initial inter-beacon distances of approximately 11, 11, 11.5, and 7 km for the shortest leg, and 15, 37, 11.5, and 12.5 km for the longest leg, respectively. Triplets A to D were deployed on multi-year ice (MYI) and labeled according to their proximity to the continental coastline: triplet A was located closest to the coastline, while triplet D was located furthest from the coastline. Position coordinates were available for all beacons in: triplet A until October 6th; triplet B until November 4th; triplet C until November 25th, and triplet D until November 3rd, yielding time intervals with durations of 28, 56, 77, and 59 days, respectively. As reported in Lukovich et al. (2011), positional accuracy of the ice beacons ranged from $\delta x = 2.5$ to 5 m based on circular and spherical error probability associated with the GPS module, while temporal accuracy was on the order of nanoseconds and thus negligible. Position accuracy for the ice mass balance buoys was less than 3m according to Garmin GPS16X-HVS product Standard GPS accuracy. The temporal resolution of the beacon data is two hours, and daily averages were calculated for the analysis and time series. Since the anticipated lifetime of the beacon batteries is at least one year, the beacon longevity may be attributed either to alternative mechanical failure or ice deformation and ridging. The data are archived long term through the Canadian Polar Data Catalogue (Buoy triplet centroid 2009 data, 2016).

Sea ice extent and ice type are examined using Environment Canada Canadian Ice Service (CIS) weekly ice charts, in addition to 12.5 km resolution Advanced Microwave Scanning Radiometer – EOS (AMSR-E) daily sea ice concentration (SIC) data. Daily and weekly maps illustrate spatial variability of sea ice concentrations in the Beaufort Sea, while also

The Cryosphere Discuss., doi:10.5194/tc-2016-219, 2016
Manuscript under review for journal The Cryosphere
Published: 30 September 2016

enabling an assessment of ice conditions in the vicinity of the triplet centroids during their evolution from September to November, 2009.

Atmospheric forcing in the form of sea level pressure (SLP), wind speed and direction, and surface air temperature (SAT) was obtained from North American Regional Reanalysis (NARR) data (Mesinger et al., 2006). Daily atmospheric forcing is derived by averaging 3-hourly NARR data in the vicinity of triplet centroids. Time series of daily-averaged sea level pressure (SLP) are then characterized into relative high (maxima) and low (minima) pressure tendencies. Time series of daily-averaged 10m NARR winds are used to characterize on-shore and off-shore winds.

3 Methods

In this section we describe methods used to compute i) triplet centroids and sudden changes in ice drift trajectories and ii) triplet areas and sea ice deformation in response to atmospheric forcing and interactions with the coastline. Presented also are diagnostics (base-to-height and perimeter-to-area ratios, Okubo-Weiss criterion, and shear-to-divergence ratios) used to characterize sea ice drift and deformation during sudden changes in ice drift paths. As is further described below, 'shock' parameters used to evaluate sudden changes in ice drift include SLP and turning angles, SAT and SIC in the vicinity of triplet centroids, in addition to NARR winds, ice drift and orientation. Each of these techniques is used to quantify sea ice drift in response to atmospheric forcing and ice-coast interactions. 'Response' parameters and diagnostics used to evaluate manifestation of sudden changes in deformation include triplet area, perimeter-to-area ratios, the Okubo-Weiss criterion, and the shear-to-divergence ratio.

3.1 Sudden changes in ice drift trajectories

Triplet centroids are calculated from the latitude/longitude coordinates of the three beacons comprising triplets A to D. Sudden changes or "shocks" in triplet centroid trajectories on daily timescales are calculated by applying a three-day running mean to centroid positions, and computing the variance after each mean calculation. The total variance is calculated as the square root of the sum of the squared latitudinal and longitudinal variances. Sudden changes are identified according to minima in the total variance time series, capturing interruptions to the ice drift path. The term "shocks" is used interchangeably with sudden change from the perspective of a 'shock-response' mechanism associated with sea ice response to atmospheric forcing and ice-coast interactions on daily timescales that forms the focus for the present study. Ice and atmospheric conditions are investigated according to the spatial and temporal evolution in ice beacon triplet centroids. Ice drift velocities for each triplet centroid, computed as outlined in Appendix A, further highlight acceleration/deceleration in the triplets during fall, 2009. Turning angles are calculated as the difference between 10 m NARR surface winds and beacon-derived ice drift.

The Cryosphere Discuss., doi:10.5194/tc-2016-219, 2016
Manuscript under review for journal The Cryosphere
Published: 30 September 2016

The Cryosphere Discussions

3.2 Lagrangian dispersion and sea ice deformation

Triplet areas were computed from recorded beacon latitude/longitude coordinates using Heron's formula $A = \sqrt{s(s-a)(s-b)(s-c)}$, where a, b, and c denote the length of the sides for each triplet, and $s = \frac{1}{2}(a+b+c)$. Error propagation analysis for the triangle area and triplet evolution according to Heron's formula yields initial error estimates on the order of $\delta_A = \frac{\delta x}{\sqrt{8A}}\sqrt{(b^2+c^2-a^2)^2a^2+(a^2+c^2-b^2)^2b^2+(a^2+b^2-c^2)^2c^2}$ ~ 0.05, 0.12, 0.04, and 0.04 km^2 for triplets A to D, respectively.

An assessment of the time rate of change in triplet area provides insight about sea ice deformation, namely the differential kinematic parameters (DKPs) of divergence (D), vorticity (V), shearing (S) and stretching (N) deformation rates. In particular, the change in area of a triangular configuration or triplet of drifters to estimate the divergence and local change in flow can be expressed as

$$D = \frac{1}{A}\frac{dA}{dt} = \frac{\partial u}{\partial x} + \frac{\partial v}{\partial y},$$

where *A* denotes the triangle area, and *u* and *v* depict the zonal and meridional components of ocean circulation or ice drift (following Molinari and Kirwan, 1975; LaCasce, 2008; Wadhams, 1989) with negative values corresponding to convergence. Similarly gradients in sea ice motion or deformation characteristics such as vorticity, shearing and stretching deformation rates can be computed from changes in the triplet area through rotation of the velocity vectors (Saucier, 1955). Comparable expressions and their relations are provided both from an oceanic perspective (Saucier, 1955; Molinari and Kirwan, 1975), and in an assessment of sea ice deformation in the Weddell Sea in Wadhams (1989) such that:

$$V = \frac{\partial v}{\partial x} - \frac{\partial u}{\partial y} = \frac{1}{A'}\frac{dA'}{dt}; u' = v \; and \; v' = -u$$

$$S = \frac{\partial u}{\partial y} + \frac{\partial v}{\partial x} = \frac{1}{A''}\frac{dA''}{dt}; u'' = v \; and \; v'' = u$$

$$N = \frac{\partial u}{\partial x} - \frac{\partial v}{\partial y} = \frac{1}{A'''}\frac{dA'''}{dt}; u''' = u \; and \; v''' = -v$$

where primes indicate 90° clockwise rotation of velocity vectors. Divergence is associated with a change in area, vorticity with a change in orientation, and shear and stretching with a change in triangle shape due to distortion (Table 2). According to the error estimates for triplet area, a threshold value for significant DKPs relative to uncertainties to ensure a sufficiently large signal to noise ratio is on the order of 10^{-6} s^{-1} for the daily timescales considered.

From the perspective of physical changes in sea ice, divergence (convergence) captures opening (closing) in the ice cover related to ice-ocean interactions and flux exchange (ridging). In the Arctic, negative (positive) vorticity depicts anticyclonic (cyclonic) circulation associated with surface winds and inertial oscillations. Negative (positive) shear captures a shape change whereby the northern triangle beacons travel west (east) relative to the southern pair without changing the triangle area. A negative stretching deformation rate (hereinafter referred to as stretching) indicates stretching along the y-

The Cryosphere Discuss., doi:10.5194/tc-2016-219, 2016
Manuscript under review for journal The Cryosphere
Published: 30 September 2016

axis (north-south), and shrinking along the x-axis (east-west), without changing the triangle orientation (i.e. stretching parallel or perpendicular to the coast).

In non-divergent flow, the triplet area is conserved so that expansion in one direction is accompanied by contraction in another direction and the triangle becomes an elongated filament (Prinsenberg et al., 1998). Changes in the aspect ratio (defined as the longest leg or base divided by the height) also describe changes in the triplet area; i.e., increasing values indicate elongation of the triplet and filamentation or stretching of the triangular configuration, while decreasing values indicate an equilateral configuration. An equilateral triangle is depicted by a base-to-height ratio of $\frac{2}{\sqrt{3}} \sim 1.155$. Furthermore, the perimeter-to-area ratio provides a signature of 'folding' in the sea ice drift cover in a manner similar to mechanical annealing whereby compression reduces the dislocation density of materials (Shan et al., 2007; Lawrence Berkeley National Laboratory, 2008). Perimeter-to-area ratios may also provide insight about floe shape and size distributions (Gherardi and Lagomarsino, 2015). Elongated triangles are captured by vanishing perimeter-to-area ratios, while an equilateral configuration is depicted by a perimeter-to-area ratio of $\sim 4\sqrt{3}/a$, where *a* is the length of the equilateral triangle side.

Relative contributions of the DKPs are monitored using the diagnostics of total deformation $D^2+S^2+N^2$ to assess distortion in the ice cover due to divergence, and the shearing and stretching deformation rates, as well as the vorticity squared V^2 to assess the rotational component (capturing influence from winds and/or inertial oscillations (Gimbert et al, 2012, albeit on shorter timescales)). The Okubo-Weiss (OW) criterion, defined as (Okubo, 1970; Weiss, 1991)

$$OW = Re(\frac{1}{4}\left(D^2 + S^2 + N^2 - V^2 + |D|\sqrt{S^2 + N^2 - V^2}\right),$$

highlights relative contributions from deformation and the rotational component. Values with OW < 0 (OW > 0) indicate flow dominated by vorticity (deformation). In order to further distinguish relative contributions from divergence, shearing and stretching deformation rates to the total deformation, the shear to divergence ratio is evaluated such that

$$\theta = arctan\left(\frac{\sqrt{S^2 + N^2}}{D}\right),$$

as a signature of sea ice stress, with implications for rheological characterizations. The shear-to-divergence ratio demonstrates spatial and temporal variability in DKPs and rheological characterizations of the sea ice cover. Values of 0, 45, 90, 135, and 180 degrees depict divergence, extension, shear, contraction, and convergence, respectively (Feltham, 2008; Fossen, 2016). Sought in this study is a cumulative assessment and narrative that describes relative contributions of deformation and vorticity using concepts from Lagrangian dispersion and three-particle dispersion in particular, rather than a comparison between different techniques. The quality of this approach is determined by consistency of results using each method that contribute to an overall account of spatiotemporal changes in sea ice drift and deformation on daily timescales.

The Cryosphere Discuss., doi:10.5194/tc-2016-219, 2016
Manuscript under review for journal The Cryosphere
Published: 30 September 2016

4 Results

In this section, we identify sudden changes in sea ice drift, and responses as manifested in sea ice deformation using shock-response diagnostics in the context of triplets A to D based on distance from the coastline. Specifically, in the first subsection, shock parameters including SLP, surface winds, SAT and sea ice conditions in the vicinity of triplets A to D are investigated. In the second subsection, sea ice responses to atmospheric forcing and ice-coastline interactions are examined in the context of triplet areas, sea ice deformation, relative sea ice deformation (i.e. deformation- or vorticity-dominated flow), and shear-to-divergence ratios. A detailed description of results is provided in the triplet observation report in Appendix B.

4.1 Identifying sudden changes in sea ice drift

Figure 1. Evolution in Triplet A to D centroid trajectories.

Trajectories for beacons deployed near 135 °W between 72 °N and 75 °N capture spatiotemporal evolution in ice beacon triplet centroids beginning in September, 2009, with triplet A located closest to, and triplet D located furthest from, the continental coastline (Figure 1). Triplets A and B, deployed near 72 °N, share two of the three beacons and are advected westwards to approximately 144 °W and 158 °W, surviving until October 7th and November 5th, respectively. Triplet C is deployed near 73 °N and is also advected westward to 162 °W, surviving until November 26th. Triplet D is deployed near 74.5 °N and traverses a shorter path southwards and westwards to 145 °W, surviving until November 4th.

From September to November, 2009, eight sudden (local) changes or “shocks” are identified based on changes in the (regional-scale) ice drift path (Figure 1 and Table 1). An initial change *e1* depicts a cusp in all centroid trajectories; a second shock *e2* depicts southwestward advection in triplets A to C and delayed southward migration in Triplet D; a third shock *e3* captures southward migration for all four triplet centroids; *e4* the onset of south and westward migration; *e5* the onset of south and northwestward migration for all triplet centroids culminating in a loop event for Triplet D centroid trajectories and following which triplet A stops recording (October 6th); *e6* depicts northwestward migration in triplets B and C, and a cusp in triplet D; *e7* northwestward migration for all triplet centroid trajectories; *e8* captures northwestward migration and a loop in triplet C and D centroid trajectories (Figure 1 and Table 1).

Figure 2a (shocks). Sudden changes in Triplet A to D centroid trajectories

Sudden changes or “shocks” in triplet centroid trajectories on daily timescales are, as previously noted, quantified by time series for total variances of the 3-day running mean triplet centroid positions, and identified according to minima in these time series (Figure 2). Noteworthy is enhanced latitudinal variance for Triplet D relative to Triplet A in late September/early October. By contrast longitudinal variance decreases with increasing distance from the coastline, evidenced in lower values

The Cryosphere Discuss., doi:10.5194/tc-2016-219, 2016
Manuscript under review for journal The Cryosphere
Published: 30 September 2016

The Cryosphere Discussions

for triplet D relative to triplet A. Successive minima for triplets C and D in *e1* indicate a sustained response to external forcing; 1 – 2-day lagged responses in triplets C and D centroids for *e2* – *e4* indicate delayed responses to external forcing and highlight an absence of temporal coherence between triplet centroids. Following mid-October, shocks associated with triplets C and D coincide with or precede triplet B responses at lower latitudes.

Figure 2b. – Sudden changes in Triplet A to D centroid trajectories and SLP

Minima in the total variances of the 3-day running mean triplet centroid positions capture sudden changes and interruptions in the ice drift field. Maxima also capture departures from the ice drift path. Comparison of SLP highs (Figure 3) and maxima in centroid position variances (Figure 2) demonstrates correspondence between both prior to 8 October and what is described below as the shear shock event (SSE) resulting in strong off-shore ice drift and deterioration in the ice cover. Similar behavior is observed in mean SLP and ice drift triplet centroid variances for all triplets until 8 October, following which SLP and centroid variance maxima are out of phase with a lag of approximately two days. A loss of spatial and temporal synchronicity in triplet B to D variance values is further observed following the SSE event.

Figure 3. – Atmospheric forcing and sea ice response – spatial variability

Mean SLP in the vicinity of triplets A to D is uniform, with some differences in the vicinity of triplet D (Figure 3). By contrast, turning angles highlight spatial variability in ice drift for intervals between high SLP regimes. Positive turning angles correspond to increasing mean SLP and negative turning angles to decreasing SLP for all but triplet D. In contrast to SLP, turning angles provide a regional characterization of differences in sea ice drift response based on distance from the coastline.

Figure 4. – NARR winds, sea ice drift and orientation – spatial variability

Winds and ice drift show coherence in ice drift for triplets A to C, and variations in triplet D (Figure 4). Orientation highlights increased free drift conditions at higher latitudes associated with triplet D relative to lower latitude triplets.

Figure 5. – SIC range and SAT – spatial variability

Surface air temperature (SAT) and sea ice concentrations (SIC) in the vicinity of triplet centroids show that SAT values less than 2 ºC are sustained following 14 September, 2009 for triplets A to D, with an interval of increased SAT near 14 October (Figure 5). SIC varies for triplets A to D, with lower concentrations to 24 September. Low SIC exists during a SLP high for triplet C near 22 September. Low SIC exists during a SLP low for triplet D during the first loop event in mid-October. Lower SIC also exists for triplet B as it approaches the ice edge in November (not shown).

4.2 Identifying responses in sea ice deformation

Figure 6 Triplet area evolution

In this section we explore sea ice dynamical (particularly deformation) responses to atmospheric forcing based on distance and orientation relative to the coastline. Differences in triplet area representative of sea ice deformation are observed in the evolution of all triplet triangles (Figure 6a). Specifically, triplet area evolution demonstrates enhanced variability in triplet B relative to triplets A, C, and D, with an increase in area near the ice edge in late October/early November (Figure 6b). An increase in triangle base is observed with decreasing distance from the coastline (i.e. higher base values for triplets A and B relative to triplets C and D). Triplet area is governed by height. Base-to-height and perimeter to area ratios illustrate an equilateral configuration near the ice edge and coastline in the early stages of evolution for triplet A, and late stages of evolution for triplet B, captured in base-to-height ratio values approaching 1.155. Stretching is observed closest to the coastline following 10 October during a consolidated ice regime (Triplet B), captured in increasing perimeter-to-area and base-to-height ratios.

Investigation of Area, DKPs, and P/A shows alternating cyclonic activity between triplets A and B to 22 September, during low SLP intervals (Figures 6 and 7). Also observed is alternating anticyclonic activity between triplets C and D to 22 September during low SLP intervals (Figure 7). Alternating S and N in triplets A and B in September depict stretching and contraction. These differences in DKPs and thus deformation events capture differences in turning angles. An increase in P/A near the ice edge is associated with annealing and folding near the ice edge (triplets D and B). Deformation events evident in area, DKPs, and P/A highlight influence from the coastline (i.e. differences in triplet B and C in October).

Figure 7. Sea ice deformation

The time rate of change in triplet area depicts sea ice drift response relative to the coastline. For triplet A, located closest to the coastline, sea ice deformation is characterized predominantly by vorticity and stretching (Figure 7). Triplet B is governed by vorticity for the duration of this triplet evolution, with contributions from shear until 10 October, and divergence and stretching following mid-October. Triplet C, located further from the coastline is characterized by vorticity in the early and late stages of triplet evolution with intermittent contributions from shear and to a lesser extent divergence during low ice concentration regimes. Located furthest from the coastline, triplet D is governed by vorticity, stretching, shear, and divergence in the early stages of development, and by vorticity and to a lesser extent shear for the duration of the triplet evolution. Results further show that sea ice deformation is smallest furthest from the coastline.

The Cryosphere Discuss., doi:10.5194/tc-2016-219, 2016
Manuscript under review for journal The Cryosphere
Published: 30 September 2016

Figure 8. Relative sea ice deformation.

Relative DKPs highlight relative contributions from external forcing associated with winds and bathymetry/distance from the coastline as manifested in vorticity and total deformation, namely the sum of divergence, shear and stretching deformation rates squared. Results show reduced total deformation with increasing distance from the coastline (Figure 8), evident in higher values for triplet A in late September that accompany a decrease in SIC, and for triplet B in October and November relative to triplets C and D. Enhanced vorticity is also observed during low ice concentration regimes, as demonstrated in comparatively high values for triplet D in September, and for triplet B in late October/early November. The Okubo-Weiss criterion provides a signature of deformation- (OW > 0) and vorticity (OW < 0)-dominated regimes. Noteworthy is the existence of vorticity-dominated flow for all triplets in the early stages of development. Intervals of divergence and deformation-dominated flow prevail for triplet B, with some instances observed for triplet A, C, and D again in the early stages of evolution. The Okubo-Weiss criterion results in particular show enhanced distortion in the (bounded) ice cover closest to the coastline, particularly following the shear shock event (SSE) and disintegration in the ice cover following the strong shear event, opening in the flaw lead (evident in reduced concentrations and increasing SAT in Figure 5) releasing heat to the atmosphere and resulting in increased SAT. Theta values illustrate changes in the ice strength due to relative contributions from divergence and the total strain rate ($S^2 + N^2$), as is discussed further below in Section 5 in the context of a prescription for identifying and describing 'shock-response' pairs.

5 Discussion

The present study is motivated by i) a characterization and understanding of correspondence between sudden changes in sea ice drift based on triplet centroids, atmospheric forcing and distance relative to the coastline on daily timescales, and ii) identifying responses in sea ice drift as manifested in sea ice deformation monitored through evolution in triplet area. In this section we discuss the results in the context of the eight identified sudden changes, in light of these guiding questions.

Sudden changes in sea ice drift occur between SLP high regimes (Figures 2 and 3 and Table 1). In particular, events *e1*, *e3*, *e4*, *e6* and *e8* occur during reversals in wind and ice drift (Figure 4). Noteworthy also are sudden changes in sea ice drift during persistent (~ 3 – 4 days) easterly to northerly winds associated with inflection points in the ice drift variance (events *e2*, *e5* and *e7* in Figure 2 and Table 1) and during SLP highs that coincide with maxima in the ice drift variance (Figures 2 and 3). Of particular interest is a sudden change on 8 October due to easterly winds during a SLP high within a high ice concentration (> 95%) ice regime, which induced strong offshore ice drift not evident in prior SLP high-induced sudden ice drift changes within lower ice concentration regimes. We hereinafter refer to this event as the 'Shear Shock Event' or 'SSE' to highlight the transition from a coupled to an uncoupled ice-atmosphere regime, as is described further below.

All events, namely those characterized by reversals in winds or persistent easterly and northeasterly winds, are accompanied by on- or offshore ice drift in response to winds, ice conditions, and interaction with the coastline. The turning

The Cryosphere Discuss., doi:10.5194/tc-2016-219, 2016
Manuscript under review for journal The Cryosphere
Published: 30 September 2016

angle, Okubo-Weiss criterion, and ratio of shear to divergence, provide a signature of ice mechanics, deformation, and ice strength inherent in the "shock-response" mechanism.

In the following we characterize sudden changes in the centroid trajectories due to wind reversals between SLP highs, including *e1*, *e3*, *e4*, *e6*, and *e8*. During *e1*, triplet A, located near the ice edge, is characterized by onshore followed by offshore ice drift accompanied by a low ice concentration regime (Figure 5), divergence (Figure 7), and a comparatively weak ice cover (lower θ in Figure 8). Triplet B exists in a low ice concentration regime (Figure 5) with weak deformation (Figure 7) governed by shear (Figure 8; $\theta \sim 90$). Further from the coastline, triplet C is distinguished by a lower ice concentration regime, with 0 < SAT < 2 °C (Figure 5), dominated by vorticity (Figure 7 and OW < 0 in Figure 8) in shear flow ($\theta \sim 90$ in Figure 8), and subsequent strengthening (Figure 8) due to convergence. Located furthest from the coastline, triplet D exists in a higher ice concentration regime (Figure 5) and a stronger ice cover ($\theta \sim 180$ in Figure 8) associated with convergence (Figure 7) due to onshore winds. Turning angle results showing large values for triplets A to C relative to D can be attributed to interference with the coastline, with energy propagating away from the coastline, thus exerting less influence on triplet D. Similarly, OW and θ results demonstrate a stronger (weaker) ice cover during offshore (onshore) winds near the ice edge for triplet B as the triplet moves away from (towards) the ice edge, while a weaker (stronger) ice cover is observed during offshore (onshore) winds for triplet D located furthest from the coastline. These results are corroborated in subsequent sudden changes.

During *e3*, coherence in triplet A to D response as the ice cover consolidates (higher and similar ice concentrations for all triplets as depicted in Figure 5) is evident in comparable turning angles for all triplets. High turning angles are observed for all triplets due to a high ice concentration regime, indicating the impact of ice interactions with the coastline. Despite comparable turning angles, differences exist between triplets in the strength associated with the shear-to-divergence ratio. DKPs and the shear-to-divergence ratio in particular capture local differences in the ice cover, showing a reduction in strength associated with reduction in ice concentrations for triplets A, C, and D during reversals between along and onshore drift. By contrast, the sudden change in triplet B is characterized by strong deformation (OW > 0; Figure 8) in the form of shear, and in the second component of sudden change in triplet C also by shear, both of which are accompanied by an increase in ice strength.

Coherence in triplet A to C behaviour during a high ice concentration regime is further demonstrated in turning angles during *e4*. Local differences are further manifested in DKPs and in the OW criterion and shear-to-divergence ratio specifically. Triplet A traverses a weaker ice cover in the transition from on- to along-shore ice drift resulting in weaker interactions with the coastline. Triplet B encounters a weaker ice cover in the transition from on-to-along shore ice drift and a vorticity- to a deformation (normal or stretching, N)-dominated regime, during which weak divergence is also observed. Triplet C experiences convergence and divergence in shear (Figure 7) resulting in a transition from uniaxial contraction to pure shear during the ice drift onshore and alongshore drift. [If influenced by ice interactions with the coastline, it would be expected for the opposite to occur, namely a relaxation in ice-coast interactions and weakening during the transition from on- to alongshore drift, followed by an increase in interactions and thicker or strengthened ice cover with subsequent on-shore drift.] By contrast, triplet D is characterized by shear (θ ~ 90 in Figure 8) despite onshore ice drift, indicating that triplet D, located furthest from the coastline, is least influenced by it.

Shear Shock Event

The Shear Shock Event (SSE) and sudden change occurs on 8 October during a maximum in the triplet centroid ice drift variance (Figure 2) and SLP high (Figure 3). Despite prior instances of correspondence between the maxima in SLP and ice drift variance, this event induces a comparatively strong offshore ice drift response to easterly winds (Figure 4), most likely due to the high ice concentration regime (> 97%) encountered by all triplets over the preceding three weeks (Figure 5), intimating a consolidated ice cover. The SSE results in shear-dominated flow for triplet B and shear-dominated flow oriented in the opposite direction for triplet C two days later (Figure 7). Strong southeasterly drift also coincides with reduced ice concentrations for triplets B, C, and D, one, three and five days following the SSE, respectively (Figures 4 and 5). The Okubo-Weiss criterion, and shear-to-divergence ratio capture the transition to a shear-dominated regime. Specifically, for triplet B, OW > 0 (Figure 8), while θ ~90 during the SSE, followed by a subsequent increase in ice strength associated with onshore ice drift in a high ice concentration regime (Figure 5). Triplet C experiences contraction associated with onshore ice drift during SSE evidenced in higher θ for triplet C (~180) than for triplet B (~90) (Figure 8), which is subsequently released by the strong shear event and accompanying opening in the ice cover (Figures 4 and 7).

In the interval following the SSE and during *e6*, turning angles coincide for triplets B and C as both migrate to a lower ice concentration regime, in contrast to triplet D located in a high ice concentration regime. Furthermore, sudden changes occur during the transition from off- to along-shore ice drift for triplets B and C, and off- to along- to on-shore ice drift for triplet D. Local differences are again observed in the DKPs, the OW criterion, and shear-to-divergence ratio diagnostics. In particular, triplet B is characterized by deformation-dominated flow (OW > 0; Figure 8) in the form of stretching in the meridional direction (N < 0; Figure 7). High θ for triplet B on 10 October suggests compression against the consolidated ice pack due to offshore ice drift, followed by successive weakening in the ice cover in the transition to alongshore ice drift. Successive deformation-dominated intervals (Figure 8) suggest continued deterioration in the ice cover encountered by the southernmost triplet B associated with increased divergence and reduced ice concentrations as the beacons approach the ice edge in the latter stages of evolution. Triplet C is characterized by a deformation–dominated ice regime following the strong southerly/southeasterly wind event (OW > 0 in Figure 8) due to westward shear (S < 0 in Figure 7) that coincides with a drop in ice concentration (Figure 5), suggesting a lead opening or crack in the ice cover. A subsequent recovery in ice concentration suggests refreezing for SAT < 0 °C, although a continued increase in temperature indicates warming of the surrounding atmosphere due to heat released through the crack in the ice cover previously encountered by triplets B and C (Figure 5). Triplet D is distinguished by decreasing ice strength that accompanies decreasing ice concentrations associated with increasing SAT (Figures 4 and 8).

During *e8*, turning angles differ for all three triplets (Figure 3). Triplet B experiences a low ice concentration regime associated with increased divergence (captured by the change in triplet area, Figure 6). During *e8*, triplet B is governed by vorticity (OW <0; Figure 8, and Figure 7) during a transition from off-shore to along-shore ice drift within ice concentrations

The Cryosphere Discuss., doi:10.5194/tc-2016-219, 2016
Manuscript under review for journal The Cryosphere
Published: 30 September 2016

ranging from less than 80% to 95%, resulting in a decreasing strength in the ice cover. Triplet C exists in a high ice concentration regime and experiences an increase in ice strength during the transition to offshore ice drift that results in compression of the consolidated ice cover against the pack ice to the north. By contrast, triplet D is distinguished by a transition from along- to offshore ice drift in a high ice concentration regime with a comparatively weak decrease in ice strength, indicating weak influence from the coastline. Noteworthy also is increasing SAT in the vicinity of triplet B and to a lesser extent C, relative to triplet D.

For sudden changes associated with persistent northerly and northeasterly winds, and inflection points in the centroid variance, namely *e2*, *e5*, and *e7,* lower turning angles are observed compared to those related to wind and ice drift reversals, with differences between triplets (Figure 3). These sudden changes are associated with strong northerly (onshore) winds that do not induce an ice drift reversal, but influence instead sea ice deformation evidenced in DKPs and changes in the shear-to-divergence ratio as a signature of ice strength. These events are characterized by predominantly alongshore ice drift.

During *e2*, coherence is observed from triplets A to C during high (~95%) ice concentration regimes. The sudden change in triplet A associated with onshore winds exhibits weak deformation in a high ice concentration regime; reduced strength in the ice cover following the sudden change occurs during meridional stretching ($N < 0$ in Figure 7). Weakening in the ice cover illustrates the location of triplet A near the ice edge and hence greater mobility. The sudden change in triplet B is associated with a transition from divergence to vorticity during onshore winds in a higher ice concentration regime (Figure 7, and $OW < 0$ in Figure 8). Changes in strength (Figure 8) further reflect a transition from divergence to vorticity, and subsequent restoration in shear, evidenced in θ~90 near 20 September. Vorticity, as a reflection of external forcing, may be considered as an interruption to the path associated with shear in the superposition of DKPs, which detracts from, rather than reinforces, ice strength. Higher (lower) P/A values during strengthened (weakened) ice cover intervals in triplet B (Figure 6), in addition to alternating vorticity for triplets A and B, and to a lesser extent C and D (Figure 7), also suggest a folding or annealing mechanism during sudden changes induced by onshore winds without inducing a change in ice drift orientation.

Triplet C experiences a sudden change during the transition from divergence to shear associated with onshore winds and lower ice concentrations, resulting in sustained shear. On 16 October, triplet D encounters a high ice concentration regime (Figure 5), precipitating strong deformation (meridional stretching, $N < 0$, Figure 7), and a sudden decrease in height and area (Figure 6). On 17 October, triplet D is governed by vorticity ($OW < 0$, Figure 7) in a lower ice concentration regime and a weaker ice cover (Figure 8). Higher compression during *e2* (higher θ values in Figure 8) is associated with onshore winds and drift, and an accompanying increase in ice concentration. Subsequent weakening is associated with a weakening in onshore winds. Higher ice concentrations further result in sustained shear and a larger turning angle compared to other triplets.

During *e5*, smaller turning angles than for the sudden events that induce ice-drift reversals are observed, with differences between triplets B, C, and D. All triplets exist in a high ice concentration regime. A transition from along- to onshore ice drift for triplets B and C accompanied by lower θ values suggests reduced strength in the ice cover near the coastline, in contrast to triplet D, which experiences a transition from on- to along-shore ice drift associated with a strengthened ice cover further from the coastline. Following SSE, and loss of synchronicity and coherence in ice-atmosphere interactions as well as amongst triplets, triplet B during the inflection point event *e7* experiences deformation (OW > 0) and increased ice strength ($\theta \sim 180$, Figure 8 and Table 3). Triplets C and D located further from the coastline exhibit weak deformation in a lower ice concentration regime in shear, and constant triplet area. Sudden changes associated with northerly winds and alongshore ice drift coincide with intervals between enhanced P/A for events *e2* and *e7* for triplet B, indicative of an annealing or folding mechanism, with event *e5* interrupted by the SSE. Simulated annealing and folding in the seasonal ice zone is evident in P/A for triplet B (no open boundary as for triplet A, yet with higher deformation compared to triplets C and D).

6 Conclusions

In this study we developed a framework for the assessment of sudden changes in sea ice drift in response to atmospheric forcing and ice-coast interactions based on beacons deployed in a triangular configuration as triplets and three-particle dispersion analyses. The diagnostics and tools developed provided a unique characterization of sea ice drift and deformation processes in the southern Beaufort Sea, with implications for quantifying "shock-response" systems relevant for ice hazard assessments and forecasting applications.

Sudden changes in sea ice drift on daily timescales provide a signature of sea ice response to atmospheric forcing. In response to our first research questions, we identified eight sudden changes captured by temporal discontinuities in the three-day running means in variances of triplet centroid positions. 'Shock' parameters used to evaluate sudden changes in ice drift included SLP and turning angles, SAT and SIC in the vicinity of triplet centroids, in addition to NARR winds, ice drift and orientation. Comparison of drift variance and SLP mean time series in the vicinity of the triplets indicate that the "shock-response" mechanism occurs with SLP gradients, while turning angles and shock events provide an initial and regional indication of sea ice mechanics and deformation due to interactions with the coastline. Winds and ice drift illustrate a shear shock event (SSE) on 8 October due to easterly winds within a high ice concentration regime, resulting in strong offshore ice drift, and subsequent loss in both ice-atmosphere synchronicity and spatial coherence in triplet events. Demonstrated also are changes in ice concentrations during sudden changes, with lower ice concentrations for all triplets during the early stages of evolution, and for triplet B following the SSE. Sudden changes reflect sea ice drift responses to SLP low and high regimes; regional differences are manifested predominantly in turning angles, the local characterizations of which are explored in an assessment of triplet area, deformation (DKPs), and relative deformation.

Sea ice deformation provides a signature of sea ice response to ice-coast interactions. In response to our second research questions, investigation of sea ice deformation events during sudden changes illustrated local changes in sea ice cover based on interactions with the coastline, and distance relative to the coastline. 'Response' parameters and diagnostics included the evolution in triplet area, perimeter-to-area ratio, the Okubo-Weiss criterion to monitor relative contributions from vorticity

The Cryosphere Discuss., doi:10.5194/tc-2016-219, 2016
Manuscript under review for journal The Cryosphere
Published: 30 September 2016

(due to external forcing) and deformation (associated with distortion in the ice cover), in addition to the shear-to-divergence ratio as a signature of sea ice stress and strength in the ice cover.

Triplet areas depict local responses due to ice strength and drift. Triplet area during sudden changes demonstrates an increase in triplet A near the ice edge, and enhanced stretching closest to the shoreline. DKPs further show that sea ice deformation is weakest furthest from the coastline. Relative DKPs highlight enhanced distortion in the (bounded) ice cover encountered by Triplet B, located closest to the coastline, particularly following the shear shock event on 8 October that led to a fragmented ice cover and reduced ice concentrations.

Results from this analysis suggest that sudden changes in the southern Beaufort Sea occur either during i) a reversal in winds that induce onshore/offshore ice drift, or ii) sustained north/easterly winds, with response mechanisms governed by ice conditions and interactions with the coastline. Regional differences in triplet events are captured by turning angles, and local differences by DKPs, the OW criterion, and shear-to-divergence ratio.

Sudden changes associated with wind reversals (minima in drift variance; *e1*, *e3*, *e4*, *e6*, and *e8*) occur during SLP gradients. Changes in ice strength evident in shear-to-divergence ratios are associated with the transition from an on or offshore to along-shore ice drift regime. Triplet D, located furthest from the coastline, is uninfluenced by ice-coast interactions. Noteworthy also is the existence of a sudden change due to easterly winds within a consolidated ice regime which induced strong offshore ice drift on 8 October and precipitated a decline in the ice cover near the ice edge encountered by triplet B.

Sudden changes associated with maxima or inflection points in ice drift variance (*e2*, *e5*, and *e7*) occur during persistent northerly/northeasterly winds. Results suggest that vorticity superimposed on shear weakens ice strength, and that following vorticity, a 'folding' occurs that appears associated with a strengthening in the ice cover, in a manner similar to mechanical annealing. Alternating cyclonic/anticyclonic regimes in triplets A and B and to a lesser extent C further suggest a folding mechanism within the bounded ice regime located closest to the coastline. These results raise the question as to whether vorticity anticipates a stronger ice cover.

Results from this analysis provide a prescription for identifying sudden changes in the ice drift field and accompanying changes in deformation characteristics based on distance from the coastline and proximity to the ice edge (where ice drifts more freely) relevant for prediction and ice-hazard detection on daily timescales. Proposed future work includes the use of the shock-response parameters, and Okubo-Weiss criterion and shear-to-divergence ratio diagnostics in particular for model-data comparison in applications involving ice hazard detection, forecasting and prediction. Numerical experiments testing sea ice response to shock events during SLP high and low regimes will provide additional insight into physical mechanisms responsible for the observed local kinematic and deformation features in the ice drift field.

The identification of two distinct categories of sudden changes or shock events (reversals and northerly/northeasterly), and conditions necessary for a strong offshore ice drift event will enable the construction of an integrated observational-modeling framework designed specifically to understand ice-atmosphere interactions in the context of drift and deformation. Also of interest is improved understanding of the simulated annealing mechanism associated with persistent northerly winds and along-shore ice drift. Furthermore, an understanding of floe size shapes and distributions prior to, during, and following sudden changes in the ice drift cover using these diagnostics, and shear-to-divergence ratio in particular, will improve our understanding of how the sea ice cover responds to atmospheric forcing based on distance from and interaction with the coastline. Results from this analysis can be applied to develop an observational-modeling framework for Lagrangian dispersion that monitors sea ice drift and deformation at large, regional, and local spatial scales. Implications for EVP and rheological characterizations of sea ice using observations, results and diagnostics from this investigation could further be explored.

Proposed work using results from this study includes efforts to address the question: What are the implications of changing ice and atmospheric patterns and dynamics for ice –atmosphere interactions, including heat and momentum exchange in particular, and local and global-scale processes more generally?

Acknowledgements

Buoy data were funded by the Natural Sciences and Engineering Research Council of Canada, the Canada Foundation for Innovation and partner organizations. Funding for this study was also provided by the Canadian Networks of Centres of Excellence (NCE) program, and Canada Research Chairs (CRC) programme (D.G. Barber). The authors would like to thank D. Babb and R. Galley for triplet deployment and for contributions to an earlier version of this manuscript. This work was completed as a contribution to the ArcticNet and Arctic Science Partnership networks.

References

Bourassa, M. A., Gille, S. T., Bitz, C., Carlson, D., Clayson, C. A., Cerovecki, I., Cronin, M. F., Drennan, W. M., Fairall, C. W., Hoffman, R. N., Magnusdottir, G., Pinker, R. T., Renfrew, I. A., Serreze, M., Speer, K., Talley, L. D., and Wick, G. A.: High-latitude ocean and sea ice surface fluxes: Challenges for climate research. Bulletin of the American Meteorological Society, 94, 3, 403-423, 2013.

Carleton, A. M.: Synoptic sea ice-atmosphere interactions in the Chukchi and Beaufort Seas from NIMBUS 5 ESMR data, J. Geophys. Res., 89, D5, 7245–7258, doi:10.1029/JD089iD05p07245, 1984.

Carmack, E., Polyakov, I., Padman, L., Fer, I., Hunke, E., Hutchings, J., Jackson, J., Kelley, D., Kwok, R., Layton, C., Melling, H., Perovich, D., Persson, O., Ruddick, B., Timmermans, M.-L., Toole, J., Ross, T., Vavrus, S., and Winsor, P.: Toward quantifying the increasing role of oceanic heat in sea ice loss in the new Arctic, Bulletin of the American Meteorological Society, 96,12, 2079-2105, 2015.

Colony, R. and Thorndike, A.S.: An estimate of the mean field of Arctic sea ice motion, J. Geophys. Res., 89, C6, 10,623–10,629, doi:10.1029/JC089iC06p10623, 1984.

Colony, R. and Thorndike, A.S.: Sea ice motion as a drunkard's walk, J. Geophys. Res., 90, C1, 965–974, doi:10.1029/JC090iC01p00965, 1985.

Geiger, C.A., Ackley, S.F., and Hibler III, W.D.: Sea ice drift and deformation processes in the western Weddell Sea, in *Antarctic Sea Ice: Physical Processes, Interactions and Variability*, Antarct. Res. Set., vol. 7, pp. 141-160, edited by M.O. Jeffries, AGU, Washington, D.C., 1998.

Geiger, C.A., Zhao, Y., Liu, A.K., and Hakkinen, S.: Large-scale comparison between buoy and SSM/I drift and deformation in the Eurasian Basin during winter, 1992 – 1993, J. Geophys. Res., 105, C2, 2257 – 3368, 2000.

Geiger, C.A. and Drinkwater, M.R.: Impact of temporal-spatio resolution on sea-ice drift and deformation, IUTAM Symposium on Scaling Laws in Ice Mechanics and Dynamics, (eds.) J.P. Dempsey and H.H. Shen, Kluwer Academic Publishers, Netherlands, 407-416, 2001.

Geiger, C. A. and Perovich, D.K.: Springtime ice motion in the western Antarctic Peninsula region, Deep-Sea Res. II, 55, 338 – 50, 2008.

Gherardi, M. and Lagomarsino, M.C.: Characterizing the size and shape of sea ice floes, Nature, Scientific Reports 5, 10226, doi: 10.1038/srep10226, 2015.

Guest P. S. and Davidson, K.L.: The aerodynamic roughness of different types of sea ice. J. Geophys. Res. 96, C3, 4709–4721, 1991.

Hakkinen, S.: Coupled ice–ocean dynamics in the marginal ice zones: upwelling/downwelling and eddy generation. J.Geophys. Res. 91, C1, 819–832, 1986.

Heil, P. and Hibler, W.D.: Modeling the high-frequency component of Arctic sea ice drift and deformation, J. Phys. Oceanography, 32, 3039 – 3057, 2002.

Heil, P., Hutchings, J.K., Worby, A.P., Johansson, M., Launiainen, J., Haas, C., and Hibler, W.D.: Tidal forcing on sea-ice drift and deformation in the western Weddell Sea in early austral summer, 2004, Deep-Sea Res., Part II – Topical studies in oceanography, 55, 8-9, 943-962, 2008.

Heil, P., Massom, R.A., Allison, I., Worby, A.P., and Lytle, V.I.: Role of off-shelf to on-shelf transitions for East Antarctic sea ice dynamics during spring 2003, J. Geophys. Res. – Oceans, 114, C09010, doi:10.1029/2008JC004873, 2009.

Heil, P., Massom, R.A., Allison, I., Worby, A.P.: Physical attributes of sea-ice kinematics during spring 2007 off East Antarctica, Deep-Sea Res., Part II- Topical studies in oceanography, 58, 9-10, 1158 – 1171, 2011.

Hutchings, J. K., Heil, P., Hibler III, W. D.: On modelling linear kinematic features in sea ice. Monthly Weather Review, 12, 3481-3497, 2005.

Hutchings, J.K., Roberts, A., Geiger, C., and Richter-Menge, J.: Spatial and temporal characterization of sea-ice deformation, Ann. Glaciol., 52,57 Pt 2, 360–368, doi: 10.3189/2011AoG57A185, 2011.

Hwang, P. A.: Temporal and spatial variation of the drag coefficient of a developing sea under steady wind-forcing. J. Geophys. Res., 110, C07024, doi:10.1029/2005JC002912, 2005.

Kwok, R. and Cunningham, G. F.: Deformation of the Arctic Ocean ice cover after the 2007 record minimum in summer ice extent, CRST, 76-77, doi: 10.1016/j.coldregions.2011.04.003, 2012.

LaCasce, J.H.: Lagrangian statistics from oceanic and atmospheric observations, Lect. Notes Phys., 744, 165-218, 2008.

Lawrence Berkeley National Laboratory (2008, January 3), Mechanical Annealing, Increased Strength and Why Materials Get Stronger as They Get Smaller. Retrieved from http://www.azonano.com/article.aspx?ArticleID=2045.

Lukovich, J., Geiger, C.A., Babb, D., Galley, R., and Barber, D.G.: Ice beacon triplet deployments in the Beaufort Sea gyre, 2009 Arctic Net Ice Beacon GPS Positions and Centroid Triplet Arrays, Centre for Earth Observation Science, Canadian Cryospheric Information Network Reference Number 12709, Polar Data Catalogue, 2016.

Lukovich, J.V., Babb, D.G., and Barber, D.G.: Ice beacon trajectories in the Arctic during the IPY-CFL study, J. Geophys. Res., doi:10.1029/2011JC007049, 2011.

Lukovich, J.V., Belanger, C., Barber, D.G., and Gratton, Y.: On coherent ice drift features in the Beaufort Sea gyre, *Deep Sea Res*., Part I: Oceanographic Research Papers, 92, 56 – 74, 2014.

Lukovich, J.V., Hutchings, J.K., and Barber, D.G.: On sea ice dynamical regimes in the Arctic Ocean, *Annals of Glaciology*, 56, 69, 323 – 331, 2015.

McPhee, M.G.: Advances in understanding ice–ocean stress during and since AIDJEX, Cold Regions Science and Technology, Volumes 76–77, 24-36, http://dx.doi.org/10.1016/j.coldregions.2011.05.001, 2012.

Mesinger, F., DiMego, G., Kalnay, E., Mitchell, K., Shafran, P.C., Ebisuzaki, W., Jovic, D., Woollen, J., Rogers, E., Berbery, E.H., Ek, M.B., Fan, Y., Grumbine, R., Higgins, W., Li, H., Lin, Y., Manikin, G., Parrish, D., and Shi, W.: North American regional reanalysis, Bulletin of the American Meteorological Society, 87, 3, 343 – 360, 2006.

Molinari, R. and Kirwan, A.D.: Calculations of differential kinematic properties from Lagrangian observations in western Caribbean Sea, J. Physical Oceanography, 5, 3, 483-491, 1975.

Okubo, A.: Horizontal dispersion of floatable particles in the vicinity of velocity singularities such as convergences, Deep Sea Res., 17, 445–454, 1970.

Overland, J., Walter, B., Curtin, T. B., and Turet, P.: Hierarchy and sea ice mechanics: A case study from the Beaufort Sea, J. Geophys. Res., 100, C3, 4559 – 4571, 1995

Polar Group, The: Polar atmosphere-ice-ocean processes: A review of polar problems in climate research, Rev. Geophys.,18, 2, 525–543, doi:10.1029/RG018i002p00525, 1980.

Prinsenberg, S.J., Fowler, G.A., van der Baaren, A.: Pack ice convergence measurements by GPS-ARGOS ice beacons, Cold Regions Science and Technology, 28, 2, 59-72, doi: 10.1016/S0165-232X(98)00013-5, 1998.

Rampal, P., Weiss, J., Marsan, D., Lindsay, R., and Stern, H.: Scaling properties of sea ice deformation from buoy dispersion analysis, J. Geophys. Res., 113, C03002, doi:10.1029/2007JC004143, 2008.

Rampal, P., Weiss, J., Marsan, D., and Bourgoin, M.: Arctic sea ice velocity field: General circulation and turbulent-like fluctuations, J. Geophys. Res., 114, C10014, doi:10.1029/2008JC005227, 2009a.

Rampal, P., Weiss, J., and Marsan, D.: Positive trend in the mean speed and deformation rate of Arctic sea ice, 1979–2007, J. Geophys. Res., 114, C05013, doi:10.1029/2008JC005066, 2009b.

Richter-Menge, J. A., McNutt, S. L., Overland, J. E., and Kwok, R.: Relating Arctic pack ice stress and deformation under winter conditions, J. Geophys. Res., 107, C10, 8040, doi:10.1029/2000JC000477, 2002.

Saucier, W.J.: Principles of meteorological analysis, University of Chicago Press, Chicago, IL, 438 pp., 1955.

Shan, Z.W., Mishra, R.K., Sayed Asif, S.A., Warren, O.L., Minor, A.M.: Mechanical annealing and source-limited deformation in submicrometre-diameter Ni crystals, Nature Materials 7, 115 – 119, 2007.

Stern H.L. and Lindsay, R.W.: Spatial scaling of Arctic sea ice deformation. J. Geophys. Res., 114, C10, C10017, doi:10.1029/2009JC005380a, 2009.

Stroeve J., Serreze M, Drobot S, Gearheard S, Holland M, Maslanik J, Meier W, and Scambos T.: Arctic sea ice extent plummets in 2007. EOS, Trans. Am. Geophys. Union 89, 13–14, doi:10.1029/2008EO020001), 2008.

Taylor, G. I.: Diffusion by continuous movements, Proc. London Math. Soc., s2-20, 196–212, doi:10.1112/plms/s2-20.1.196, 1921.

Thorndike, A. S.: Kinematics of sea ice, The Geophysics of Sea Ice, NATO ASI Ser., Ser. B, 146N. Untersteiner, Plenum, New York., 489–549, 1986.

Wadhams et al.: Basin-scale ice motion and deformation in the Weddell Sea in winter, Annals of Glaciology, 12, 178 – 186, 1989.

Weiss, J.: The dynamics of enstrophy transfer in two-dimensional hydrodynamics, Physica D, 48, 273–294, 1991.

Weiss, J.: Drift, deformation, and fracture of sea ice, Springer Briefs in Earth Sciences, Springer Netherlands, Dordrecht Netherlands, doi:10.1007/978-94-007-6202-2 5, 2013.

The Cryosphere Discuss., doi:10.5194/tc-2016-219, 2016
Manuscript under review for journal The Cryosphere
Published: 30 September 2016

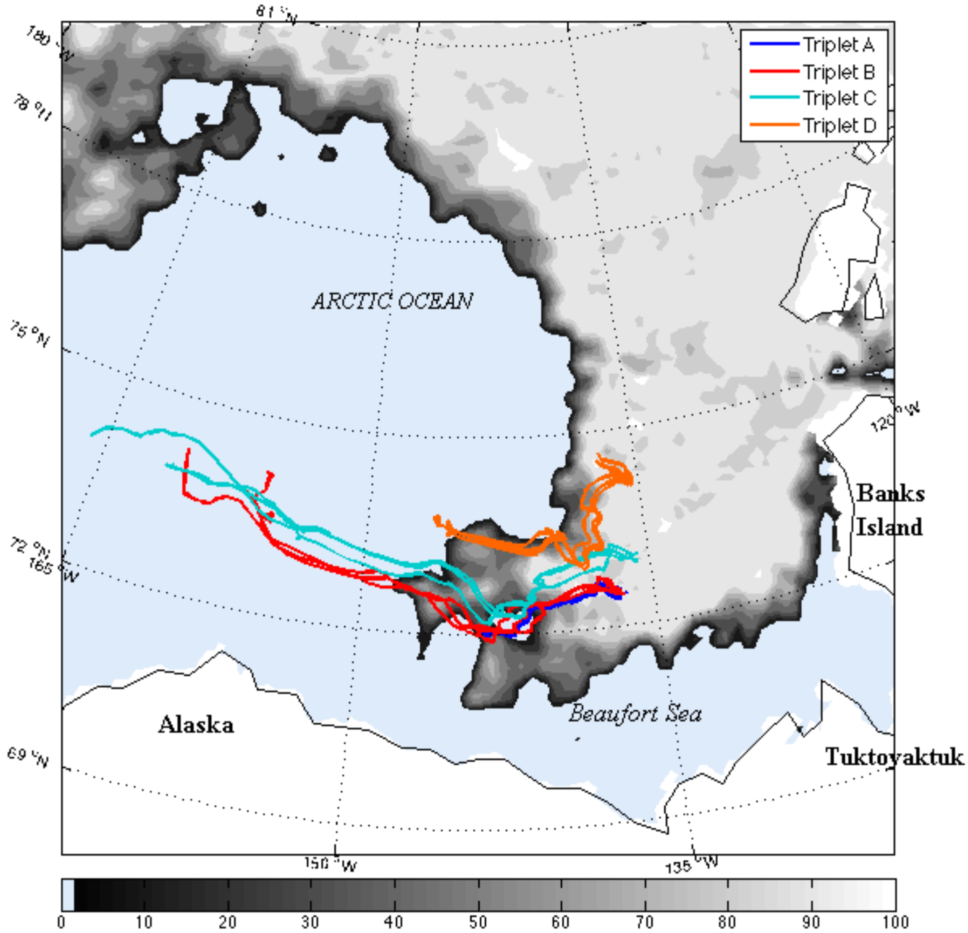

Figure 1a: GPS buoy-array-triplet trajectories relative to sea ice and coastline. Evolution in triplet A to D centroid trajectories, superimposed on sea ice concentration map in early September, 2009 on triplet deployment, with triplet A located closest to the coastline, and triplet D located furthest from the coastline. Triplet D is also initially located nearest the tongue of multiyear ice edge.

The Cryosphere Discuss., doi:10.5194/tc-2016-219, 2016
Manuscript under review for journal The Cryosphere
Published: 30 September 2016

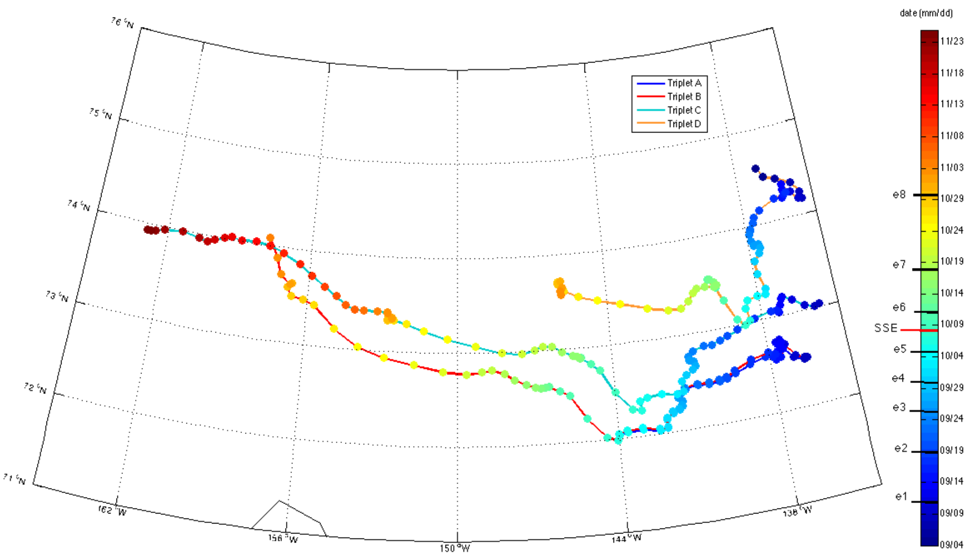

Figure 1b: Temporal evolution of triplet centroids A to D, colour-coded by date with each shock event enumerated in the colourbar timeline. The Shear Shock Event (SSE) associated with easterly winds during a SLP high and high ice concentration regime, resulting in strong offshore ice drift, and decoupling in ice-atmosphere interactions is also depicted.

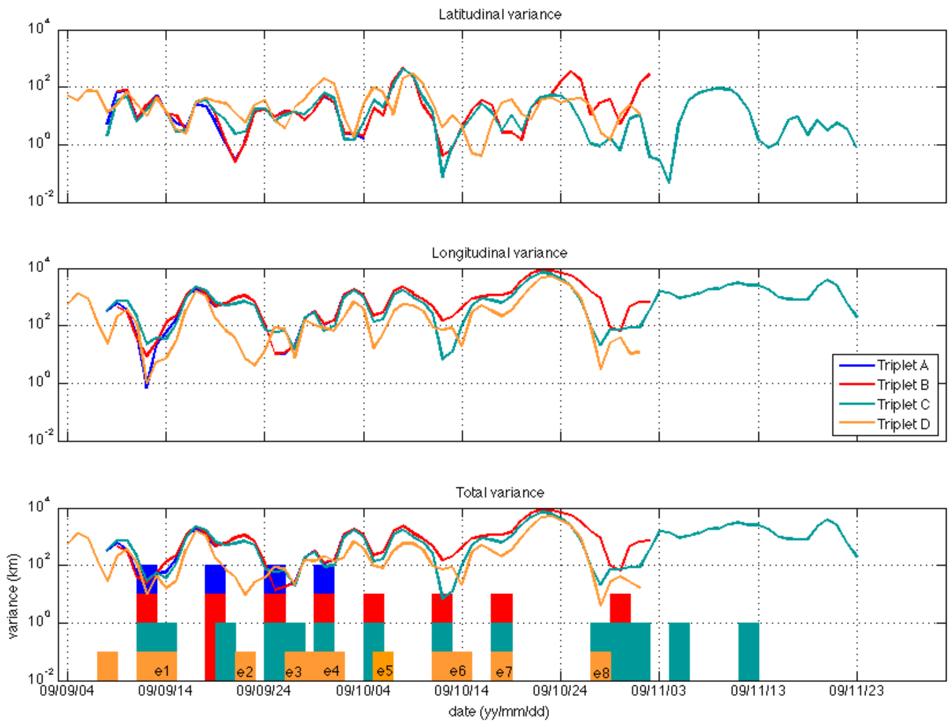

Figure 2: Abrupt changes in triplet A to D centroid trajectories, defined as minima in the variances of the 3-day running mean triplet centroid positions. The upper, middle, and lower panels depict latitudinal, longitudinal and total variance, respectively. SSE depicts the shear shock event associated with strong offshore ice drift. Comparison with mean SLP in the vicinity of the triplets shows correspondence between SLP and drift variance maxima prior to SSE; minima occur between SLP and variance maxima.

The Cryosphere Discuss., doi:10.5194/tc-2016-219, 2016
Manuscript under review for journal The Cryosphere
Published: 30 September 2016

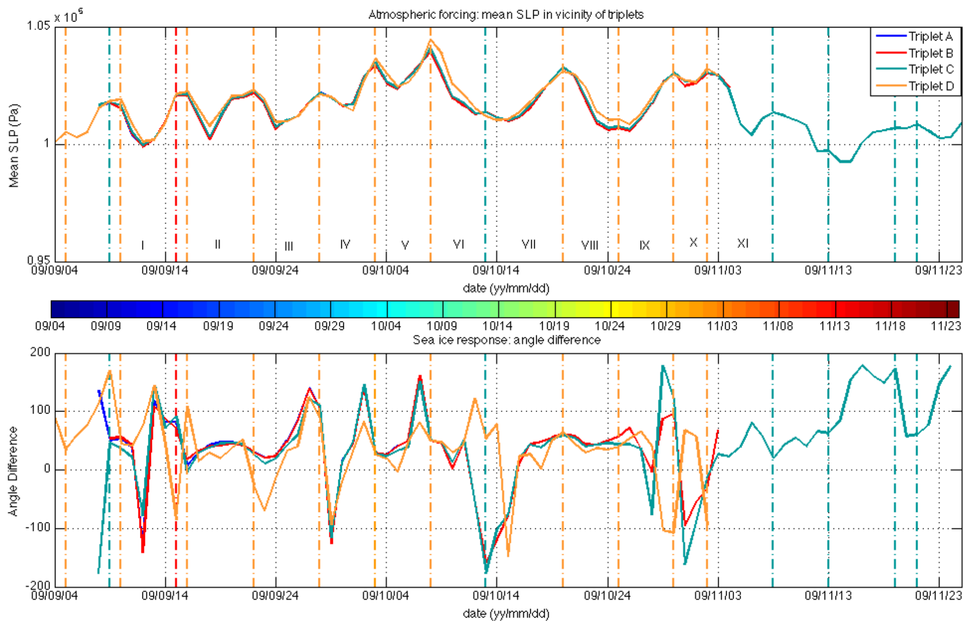

Figure 3: Atmospheric forcing and regional sea ice response. Mean SLP in the vicinity of triplets A to D highlighting atmospheric forcing (upper panel). Turning angle between surface winds and triplet centroid drift depicting sea ice response (lower panel). Colour bar indicates colours associated with centroid dates in Figure 1b.

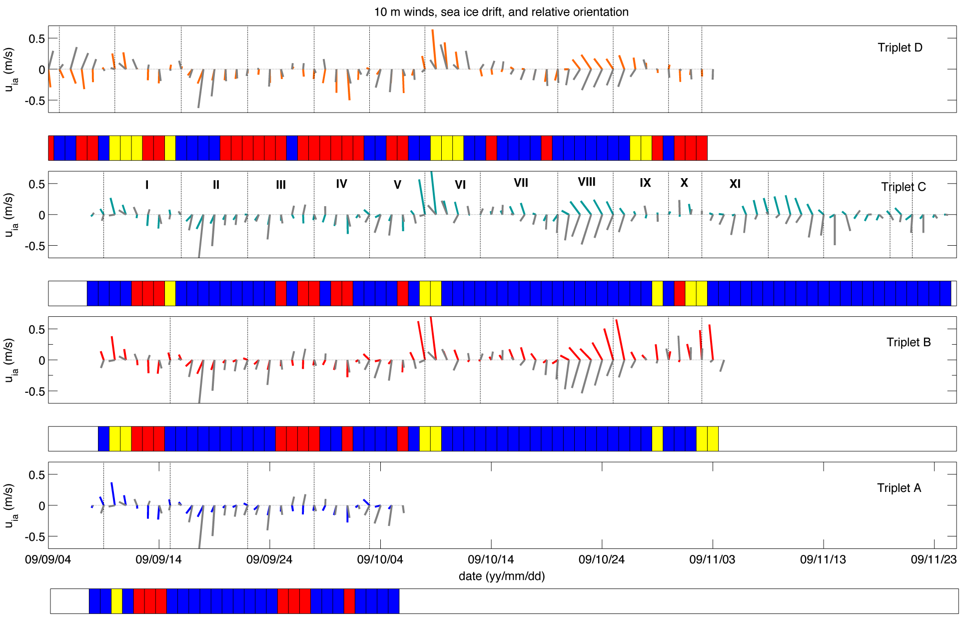

Figure 4: Winds, sea ice drift and orientation relative to the coastline. Time series of 10 m North American Regional Reanalysis (NARR) winds in the vicinity of the triplet centroids (grey vectors), sea ice drift for triplets A (lowermost panel) to D (uppermost panel), and offshore (yellow), onshore (red), and alongshore (blue) ice drift orientation.

The Cryosphere Discuss., doi:10.5194/tc-2016-219, 2016
Manuscript under review for journal The Cryosphere
Published: 30 September 2016

The Cryosphere
Discussions
Open Access

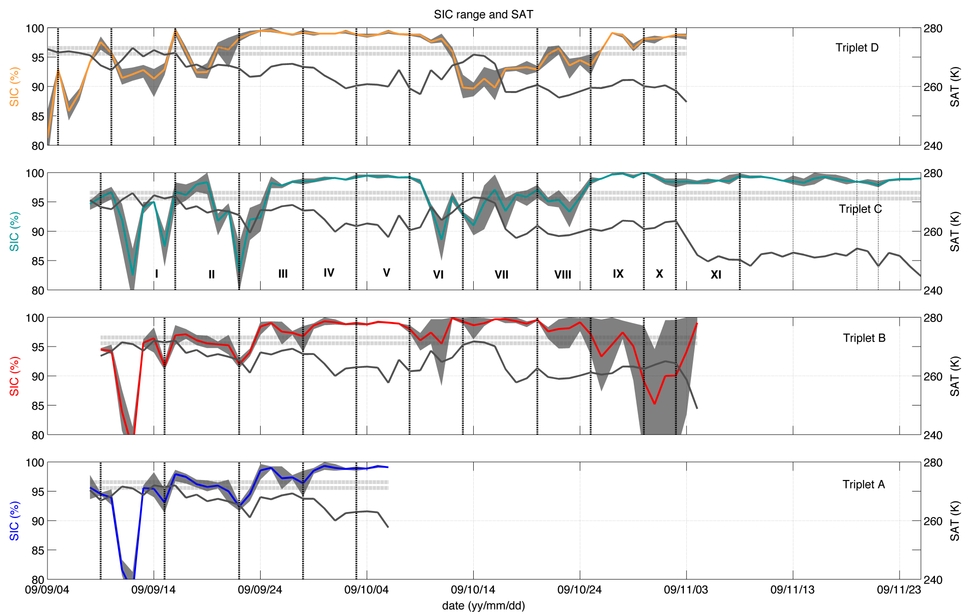

Figure 5: Sea ice concentration (SIC) range and Surface Air Temperatures (SAT). Time series of percent sea ice concentration and SAT for triplets A (lowermost panel) to D (uppermost panel). Vertical lines depict dates associated with SLP highs and roman numerals the SLP interval described in Table 3. Grey shading shows the range of ice concentrations encountered by three beacons comprising the triplets. Horizontal lines depict SAT values of 273 K and 275 K.

The Cryosphere Discuss., doi:10.5194/tc-2016-219, 2016
Manuscript under review for journal The Cryosphere
Published: 30 September 2016

The Cryosphere
Discussions
Open Access

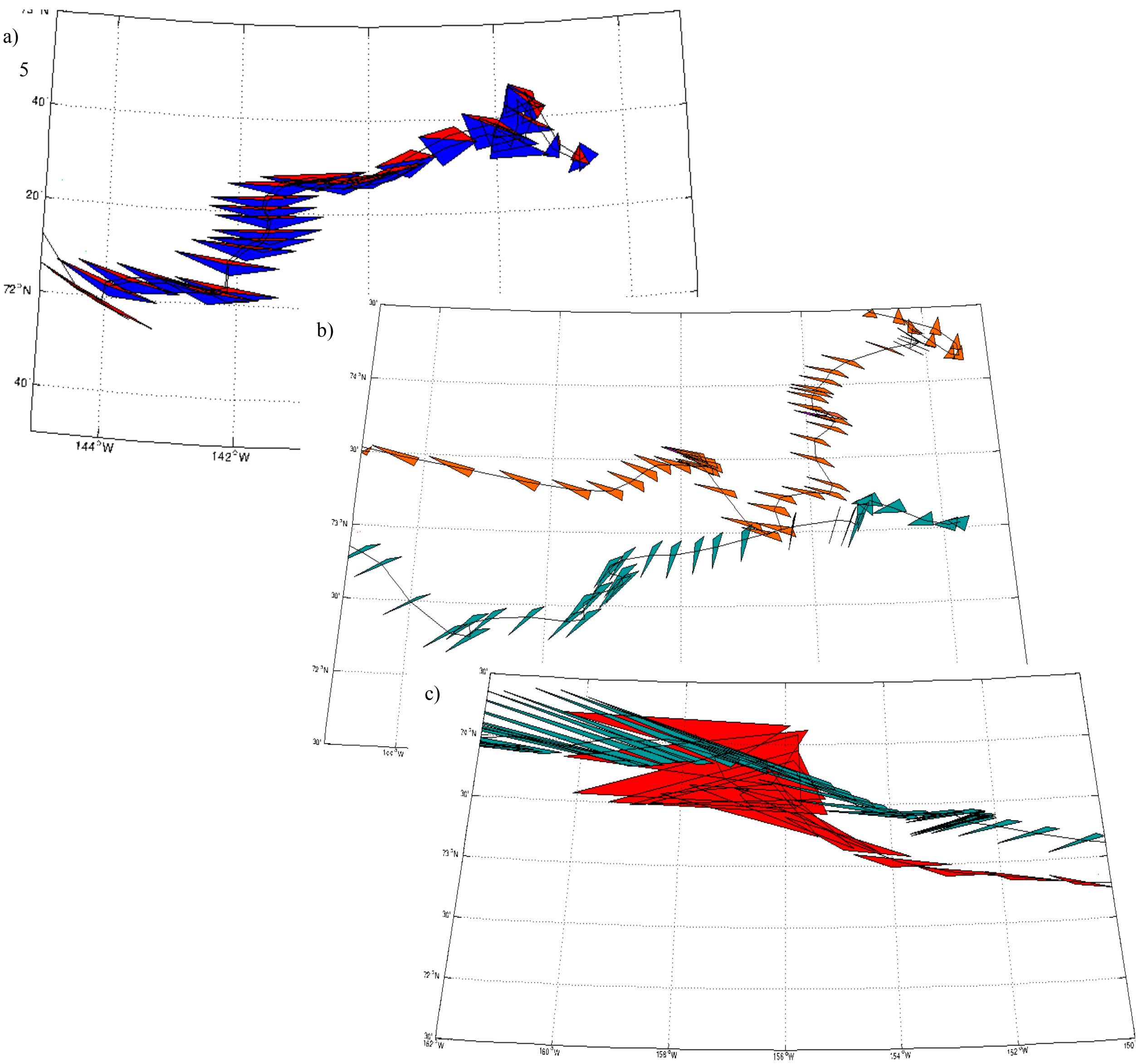

Figure 6a: Triplet area evolution. Examples of triplet evolution, including (a) initial evolution in triplets A and B, (b) evolution in triplets C and D, (c) final evolution in triplets B and C.

The Cryosphere Discuss., doi:10.5194/tc-2016-219, 2016
Manuscript under review for journal The Cryosphere
Published: 30 September 2016

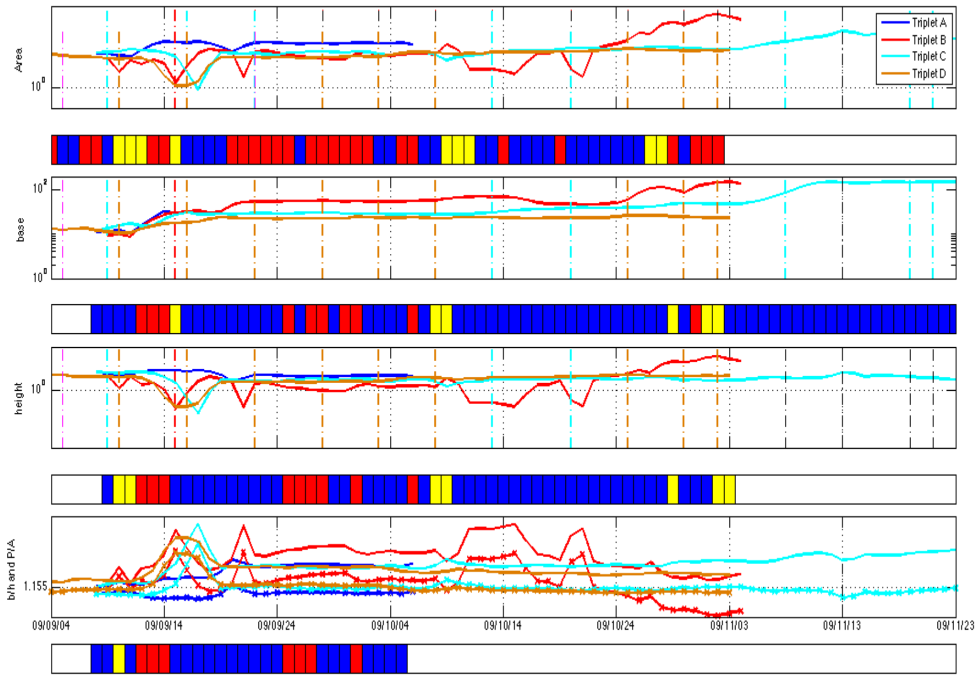

Figure 6b: Triplet area evolution. Time series of triplet area, base, height, base-to-height and perimeter-to-area ratios for triplets A to D. Solid lines in lower panel depict the base-to-height ratio, while the lines with symbols depict the perimeter-to-area ratio. The value for the base-to-height ratio associated with an equilateral configuration (1.155) is also shown. Horizontal bar graphs depict on-, along-, and offshore ice drift as depicted in Figure 5.

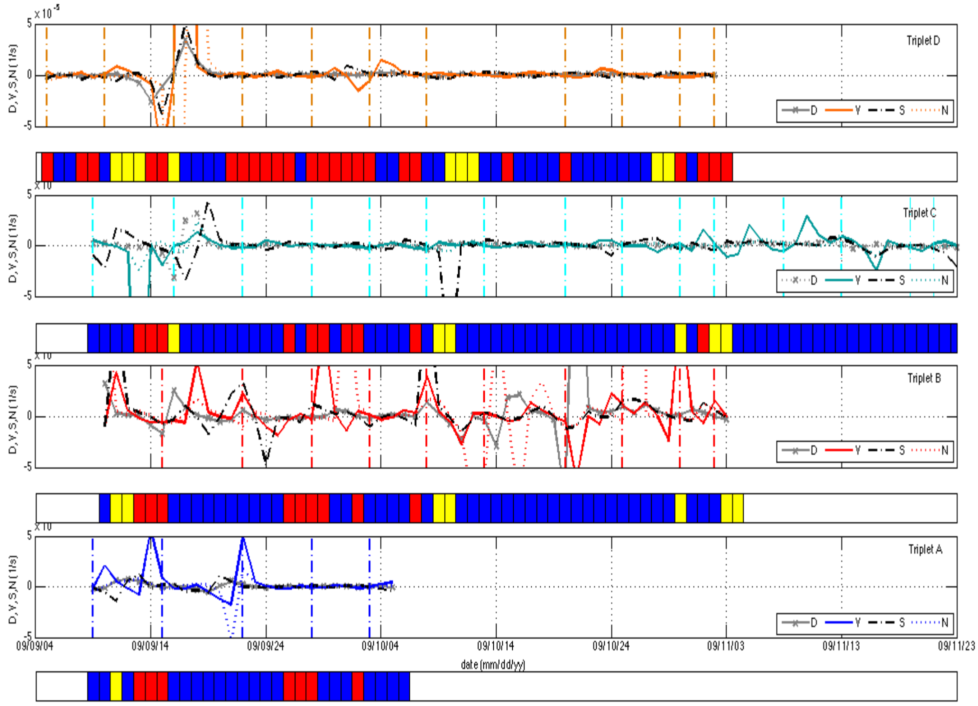

Figure 7: Sea ice deformation. Time series of Differential Kinematic Parameters (DKPs) divergence (D), vorticity (V), the shearing deformation rate (S), and the normal (stretching) deformation rate (N) for triplets A (lowermost panel) to D (uppermost panel). Vertical lines depict SLP high in the vicinity of each triplet centroid as shown in Figure 3. Horizontal bar graphs depict on-, along, and offshore ice drift as depicted in Figure 5.

The Cryosphere Discuss., doi:10.5194/tc-2016-219, 2016
Manuscript under review for journal The Cryosphere
Published: 30 September 2016

The Cryosphere
Discussions

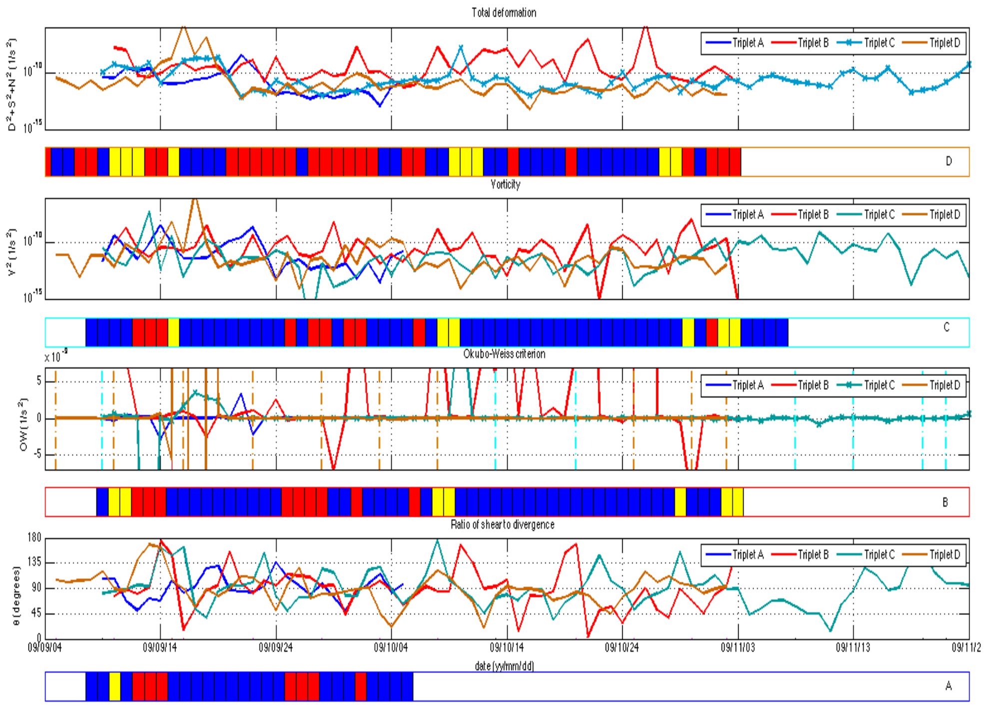

Figure 8: Figure 8: Relative sea ice deformation. Time series of relative sea ice deformation for Triplets A to D, including the total deformation ($D^2 + S^2 + N^2$), vorticity (V^2), Okubo-Weiss criterion capturing relative contributions of deformation and vorticity with OW > 0 indicating deformation-dominated flow and OW <0 indicating flow dominated by vorticity, and θ, or the arctan of the shear-to-divergence ratio to further distinguish deformation between shear and divergence-dominated regimes relevant for rheological characterizations.

The Cryosphere Discuss., doi:10.5194/tc-2016-219, 2016
Manuscript under review for journal The Cryosphere
Published: 30 September 2016

The Cryosphere Discussions

Table 1: Evolution in triplet A to D trajectories; triplet event dates and coordinates

Event/Triplet	Date (mm/dd)		Latitude		Longitude	
e1 – Initial "shock" and cusp in trajectory						
A	09/11	09/13	72.68	72.71	-137.47	-137.64
B	09/11	09/13	72.76	72.65	-137.34	-137.47
C	09/11	09/13	73.14	73.18	-136.74	-137.14
D	09/13	09/15	73.18	73.04	-137.14	-137.32
	09/11	09/13	74.26	74.36	-135.89	-136.18
	09/13	09/15	74.36	74.22	-136.18	-136.25
e2 – Second shock and southwestward migration						
A	09/18	09/20	72.57	72.46	-138.78	-139.72
B	09/18	09/20	72.65	72.62	-138.73	-139.74
C	09/19	09/21	72.96	72.88	-139.02	-139.75
D	09/21	09/23	74.02	73.95	-137.68	-137.84
e3 – Third shock and southward migration						
A	09/24	09/26	72.43	72.33	-141.34	-141.61
B	09/24	09/26	72.48	72.45	-141.37	-141.64
C	09/24	09/26	72.82	72.72	-140.87	-141.07
D	09/26	09/28	72.72	72.65	-141.07	-140.86
	09/26	09/28	73.78	73.75	-137.80	-137.55

The Cryosphere Discuss., doi:10.5194/tc-2016-219, 2016
Manuscript under review for journal The Cryosphere
Published: 30 September 2016

Event/Triplet	Date		Latitude		Longitude	
e4 – Fourth shock and south- and westward migration						
A	09/29	10/01	72.22	72.14	-141.64	-142.15
B	09/29	10/01	72.39	72.32	-141.67	-142.17
C	09/29	10/01	72.62	72.52	-140.96	-141.44
D	09/28	09/30	73.75	73.62	-137.55	-137.89
	09/30	10/02	73.62	73.32	-137.89	-137.65
e5 – Fifth shock and northwestward migration						
A	--	--	--	--	--	--
B	10/04	10/06	72.32	72.24	-143.09	-144.00
C	10/04	10/06	72.41	72.36	-142.24	-143.10
D	10/05	10/07	73.23	73.02	-138.46	-138.47
e6 – Sixth shock and northwestward migration ; triplet D loop						
A	--	--	--	--	--	--
B	10/11	10/13	72.21	72.06	-146.08	-146.63
C	10/11	10/13	72.82	72.88	-144.83	-145.22
D	10/11	10/13	73.43	73.54	-139.63	-139.83
	10/13	10/15	73.54	73.47	-139.83	-139.57

The Cryosphere Discuss., doi:10.5194/tc-2016-219, 2016
Manuscript under review for journal The Cryosphere
Published: 30 September 2016

Event/Triplet	Date		Latitude		Longitude	
e7 – Seventh shock and northwestward migration						
A	--	--	--	--	--	--
B	10/17	10/19	72.07	71.98	-147.77	-148.65
C	10/17	10/19	72.97	73.04	-145.89	-146.62
D	10/17	10/19	73.46	73.42	-140.04	-140.55
e8 – Eighth shock and northwestward migration; triplet C and D loop						
A	--	--	--	--	--	--
B	10/29	10/31	72.61	72.60	-156.67	-156.68
C	10/27	10/29	73.33	73.33	-152.50	-152.76
D	10/29	10/31	73.33	73.36	-152.76	-152.58
	10/27	10/29	73.61	73.71	-145.68	-145.92

The Cryosphere Discuss., doi:10.5194/tc-2016-219, 2016
Manuscript under review for journal The Cryosphere
Published: 30 September 2016

Table 2: DKPs and impact on triangles

Triangle feature	DKPs			
	D	V	S	N
Area	D	x*	x	
Orientation	x	V		x
Shape	x	x	S	N

*x indicates that the DKPs do not change the triangle feature

The Cryosphere Discuss., doi:10.5194/tc-2016-219, 2016
Manuscript under review for journal The Cryosphere
Published: 30 September 2016

The Cryosphere
Discussions
Open Access
EGU

Table 3: Shock-response parameters

SLP interval and triplet event	Abrupt change date	SLP	winds	Ice drift	SAT	SIC	Area, Okubo-Weiss criterion, and Shear-to-Divergence Ratio		
I and e1									
A	09/11-13	Low	SE->S	along/on	< 2°C	< 80%	Inc.	≤ 0	[90,45,90]
B	09/11-13	Low	SE->S	Off/on	< 2°C	< 80%	Const.	~0	~90
C	09/11-13	Low	SE->S	Along/on	< 2°C	~80%	Const.	≤ 0	~90
D	09/13-15	Inc	S->N	On/off	< 2°C	~95->85%	Const.	≤ 0	[90,180,135]
	09/11-13	Low	SE->S	off/on	< 2°C	~90%	Dec.	~0	[90,180]
	09/13-15	inc	S->N	On/off	< 2°C	~90%	Dec.	≤ 0	[180,90]
II and e2									
A	09/18-20	Inc	N	Along	< 0°C	~95%	Dec	~ 0	[135,90]
B	09/18-20	Inc	N	Along	< 0°C	~95%	Const	≤ 0	[90,135]
C	09/19-21	Inc	N	Along	< 0°C	~95->90%	Const	≥0	~90
D	09/21-23	LH	N	onshore	<0°C	95->100%	const	~0	[135,90]
III and e3									
A	09/24-26	Inc	N->S	Along/on	<0°C	100->95%	Const	~0	[135,90]
B	09/24-26	Inc	N->S	Along/on	<0°C	100->95%	Dec	≥0	[90,135]
C	09/24-26	Inc	N->S	Along/on	<0°C	90->97%	Const	~0	[90,45,90]
D	09/26-28	Inc	S->N	On	<0°C	~97%	Const	~0	[90,135]
	09/26-28	Inc	S->N	On	<0°C	~100%	const	~0	[135,90]

The Cryosphere Discuss., doi:10.5194/tc-2016-219, 2016
Manuscript under review for journal The Cryosphere
Published: 30 September 2016

SLP interval and triplet event	Abrupt change date	SLP	winds	Ice drift	SAT	SIC	Area, Okubo-Weiss criterion, and Shear-to-Divergence Ratio		
IV and e4									
A	09/29-01	Dec	S-> N	along/on	< 0°C	~100%	Const	~0	[90,45,90]
B	09/29-01	Dec	S->N	Along/on	< 0°C	~100%	Inc	≤0,≥0	[90,45,90]
C	09/29-01	Dec	S->N	Along/on	< 0°C	~100%	Const	~0	[135,90]
D	09/28-30	Dec	N,S,N	On	<0C (T inc)	~100%	Const	~0	~90
	09/30-02	Low	N	On	<0°C	~100%	const	~0	~90
V and e5									
A	--	--	--	--	--	--	--	--	--
B	10/04-06	Low	N	Along/on	<0°C	~100%	Inc	~0	[90,45,90]
C	10/04-06	Low	N	Along/on	<0°C	~100%	Inc	~0	[90,45,90]
D	10/05-07	Inc	N	On/along	<0°C	~100%	inc	≤0	[45,135]
Shear shock event									
VI and e6									
A	--	--	--	--	--	--	--	--	--
B	10/11-13	Low	S->N	Along	<0C (T inc)	90 – 100%	Const	≥0	~90
C	10/11-13	low	S->N	Along	<0C (T inc)	85,95,90%	Inc	~0	[45,90]
D	10/11-13	Dec	S->N	Off/along	<0C (T inc)	97 –> 90%	Inc	~0	[0,90]
	10/13-15	Low	N->S	Along/on	~0°C		const	~0	~90

The Cryosphere Discuss., doi:10.5194/tc-2016-219, 2016
Manuscript under review for journal The Cryosphere
Published: 30 September 2016

SLP interval and triplet event	Abrupt change date	SLP	winds	Ice drift	SAT	SIC	Area, Okubo-Weiss criterion, and Shear-to-Divergence Ratio		
VII and e7		--	--	--	--	--	--	--	--
A	--	Inc	NE	Along	< 0°C	~100%	Inc.	≥0	[90,180]
B	10/17-19	Inc	NE	Along	< 0°C	92-> 95%	const	~0	[45,90]
C	10/17-19	Inc	NE	Along/on	< 0°C	~92%	const	~0	[45,90]
D	10/17-19								
VIII									
A	--	--	--	--	--	--	--	--	--
B									
C									
D									
IX, X and e8									
A	--	--	--	--	--	--	--	--	--
B	10/29-31	high	N->S	Off/along	<0°C	95->80%	Inc	≤0	[45,90]
C	10/27-29	Inc	N	Along/off	<0°C	~100%	Const	~0	[90,135,90]
D	10/29-31	High	N->S	Off/on	<0°C	~100	Const	~0	[90,135]
	10/27-29	inc	N->S	Off/on	<0°C	100->95%	const	~0	~90

SLP intervals and abrupt change events defined by minima in centroid drift variance. Yellow rows depict inflection points in drift variance time series. Red row depicts SSE associated with strong offshore drift event and shear.

The Cryosphere Discuss., doi:10.5194/tc-2016-219, 2016
Manuscript under review for journal The Cryosphere
Published: 30 September 2016

Appendix A: Methodology to Derive Daily Positions, Triplet Arrays, Centroids, and Ice Drift from Telemetry Data

Geographical positions are recorded from global positioning (GPS) beacons explained in the data section. The observed temporal resolution of the beacon position data is two hours (dt = 2 hours). Daily average positions are calculated for the analysis and time series. The position data is subsequently used to compute drift components based on triplet centroid daily displacements.

A.1. Sea ice drift and triplet centroids

A four-step process was used to convert telemetry geographical position records into daily beacon averages, centroid locations, and sea ice drift. First, daily average positions were calculated from the two-hourly data for each beacon. Second, triplets were organized based on proximity to the coastline, inter-beacon distances, and overlapping time intervals. Triplets A and B, with two shared beacons, were selected to highlight differences in ice drift and deformation on scales comparable to inter-beacon separations.

Third, centroids are calculated using the coordinates of the three beacons comprising each triplet. Fourth, ice drift is computed from centroid displacements. Specifically, the geographical latitude and longitude decimal degrees are converted to horizontal ortho-linear metric distances, using the north polar azimuthal equal-area map centred on the North Pole. Thus for the Earth's radius $R = 6371.228\ km$, pixel size $C = 25.0675\ km$, latitude ϕ, longitude λ, row and column origin $r0 = s0 = 181$ for a $361x361$ grid, and

$$r = 2R \sin\lambda \sin\left(\frac{\pi}{4} - \frac{\phi}{2}\right)$$
$$s = -2R \cos\lambda \sin\left(\frac{\pi}{4} - \frac{\phi}{2}\right),$$

the speeds associated with the metric distances, $u_r = 10^3 \Delta r/(\Delta t)$ and $u_s = 10^3 \Delta s/(\Delta t)$, for $\Delta t = 24 \times 3600$(s), are transformed to zonal and meridional components such that

$$u = u_r \cos\lambda + v_r \sin\lambda$$
$$v = -u_r \sin\lambda + v_r \cos\lambda.$$

Appendix B: Triplet Observation Report

A description of observations and results determined from shock-response diagnostics is provided in this appendix as supplementary material to the results section. Results are categorized according to i) shock diagnostics (SLP, turning angle, surface winds, ice drift, SIC and SAT as depicted in Figures 3 to 5) used in identifying trajectory changes in ice drift paths, and ii) response diagnostics (triplet Areas, DKPs, relative DKPs and shear-to-divergence ratios as depicted in Figures 6 to 8) used in identifying sea ice deformation responses during sudden changes in ice drift paths.

B.2.1 Identifying trajectory changes in sea ice drift and deformation

Figure 3. – Atmospheric forcing and sea ice response – spatial variability

In the context of ice shock events, large turning angles are observed for triplets A, B, and C during a SLP low for shock *e1*. Shock events evident during a transition in SLP phase are also observed in turning angles for all triplets (Figures 2b and 3). Specifically, angle differences on the order of 40 degrees are observed during decreasing SLP for shock *e2*. Turning angles increase during a transition to a SLP high for *e3*, whereas for shock *e4* negative turning angles exist for decreasing SLP. A SLP low is observed between successive SLP highs when triplet A stops recording during *e5*. The triplet D centroid loop event during *e6* is manifested in differences in turning angles during a SLP low, in a manner distinct from other triplet turning angles. Slight differences in turning angles are observed during increasing SLP for *e7*. As for *e6*, differences in turning angles highlight spatial (relative to distance from the coastline) differences in sea ice response to external forcing as a SLP high enters the region in the vicinity of the beacon triplets. SLP mean time series in the vicinity of the triplets indicate that the “shock-response” mechanism occurs with SLP gradients and a transition between local SLP high and low regimes. As will later be explored, turning angles and shock events additionally provide an initial indication of sea ice mechanics and deformation.

Figure 4. – NARR winds, sea ice drift and orientation – spatial variability

A southerly to northerly transition in 10 m winds is accompanied by onshore ice drift for triplets A to C, and a second reversal from northerly to southerly winds accompanied by offshore ice drift for triplet D during *e1 (Figure 4)*. Strong northerly flow is observed in the vicinity of all triplets with alongshore (southwestward) drift in triplet A to C centroids, and onshore drift in triplet D during *e2*. Reversals in 10 m winds are observed with accompanying alongshore/onshore ice drift

The Cryosphere Discuss., doi:10.5194/tc-2016-219, 2016
Manuscript under review for journal The Cryosphere
Published: 30 September 2016

The Cryosphere Discussions Open Access EGU

during *e3*. An interruption to the centroid trajectory is further observed during reversals in 10 m winds during *e4*, with along-shore and predominantly onshore drift for triplet D. By contrast, dominant northerly winds result in along-shore flow for all centroids during *e5*. Reversals in 10 m winds in the vicinity of triplets B and C with accompanying alongshore flow, and predominantly southerly winds in the vicinity of triplet D during a loop event highlight regional and local responses during *e6*. Northeasterly winds and alongshore ice drift for triplets B and C, and onshore drift for triplet D further highlights local responses during *e7*. Differences in winds and drift response are again observed during shock event *e8*.

Figure 5. – SIC range and SAT – spatial variability

In consideration of shock events, SIC values of ~80% with SAT less than zero degrees Celsius are observed for triplets A and B; SIC values of ~80% and ~90% with SAT less than two degrees Celsius are observed for triplets C and D respectively during *e1*. SIC ranges from 90 – 100 % and SAT is less than two degrees Celsius for all triplets during *e2*. Similarly during *e3*, SIC ranges from 95 – 100 % with SAT < 0 for all triplets. SIC approaches 100% concentration with SAT < 0 for shock events *e4* and *e5*. Lower ice concentrations for *e6* followed by an increase in SAT suggest an opening of leads in the vicinity of triplets B and C. A delayed response is observed for triplet D. During *e7* equilibration in SAT is accompanied by SIC values ranging from 90 – 100% for triplets B, C, and D. By contrast, during *e8* SIC values are less than 80% as SAT increases for triplet B near the ice edge, while triplets C and D approach 100% ice concentration as SAT equilibrates and continues to decrease, respectively.

B.2.2 Identifying responses in sea ice deformation

Figure 6 Triplet area evolution

An assessment of evolution in triplet area during each of the sudden changes demonstrates an increase in triplet A area near the ice edge in contrast to decreasing areas for all other triplets during *e1*, with a lagged response in the maxima (Figure 6). The greatest stretching is also observed closest to the coastline. During *e2*, the base for triplets A and B increases during consolidation following which a maximum is achieved on the 21st (~ 2-day time lag). By contrast, P/A and b/h are approximately constant for triplets C and D, indicating that the triangle maintains its shape further from the continental coastline. Triplets A, C, and D maintain their shape during *e3*, while triplet B area decreases as the height decreases (P/A and b/h increase). During *e4*, P/A and b/h are constant for triplets A, C, and D with higher values further from the coastline (associated with smaller areas). A decline in P/A and b/h due to restoration in height is observed for triplet B. During *e5*, the area and ratios are approximately constant for all triplets, following which triplet A beacons stop recording. The greatest stretching (high base and ratio values) is observed in triplet B located closest to the shoreline/continental coastline. The area

The Cryosphere Discuss., doi:10.5194/tc-2016-219, 2016
Manuscript under review for journal The Cryosphere
Published: 30 September 2016

The Cryosphere Discussions

in triplet B decreases during *e6* associated with a decrease in height, resulting in increasing b/h and P/A, while triplets C and D are approximately constant. During *e7* an increase in area for triplet B is associated with an increase in height so that b/h and P/A decrease, while once again triplet C and D exhibit comparable behavior. During *e8*, triplet B approaches an equilateral configuration as the beacons approach the ice edge; increased stretching is observed for triplet C relative to triplet D continues. P/A and b/h thus provide a signature of stretching and ice drift response to the coastline, the relative contributions of which are further described by deformation and DKPs.

Figure 7. Sea ice deformation

Sea ice deformation during sudden changes highlights differences in sea ice response based on distance from the continental coastline. In particular, during *e1* triplet A is characterized by dominant contributions from vorticity, shear, and to a lesser extent, divergence, whereas triplet B witnessed a decline in shear and vorticity. Triplet C witnessed a decline in shear and transition to predominantly anticyclonic activity accompanied by comparatively weak stretching, while triplet D experienced a transition to convergence and negative vorticity. During *e2*, Triplet B experiences a transition from vorticity and stretching to shear, while triplet C is governed by shear. DKPs for triplets A and D are comparatively weak. During *e3*, only triplet B exhibits a transition from shear to anticyclonic activity, in contrast to comparatively weak DKPs for all other triplets. It should be noted that a negative stretching deformation rate indicates stretching along the y-axis (meridional) and shrinking along the x-axis (zonal). Triplet B during *e4* is characterized by a transition from cyclonic activity to stretching along the x-axis, while triplet D is distinguished by vorticity and shear compared to triplets A and C, which exhibit weak deformation. Similarly during *e5*, weak DKPs are observed for triplet C, with triplets B and D governed by vorticity. During *e6*, triplet B is governed by meridional stretching, followed by zonal stretching and oscillatory motion in N until *e7* and 20 October, following which convergence and divergence dominate. During *e8*, triplet B is governed by vorticity associated with reversals in drift orientation, while triplet C is governed by weak DKPs, following which alternating cyclonic and anticyclonic circulation is observed.

Figure 8. Relative sea ice deformation.

It is interesting to note that extrema in the Okubo-Weiss criterion roughly coincide with sudden changes in ice drift (Figure 8). In particular, during *e1*, triplet A is characterized by vorticity, while triplets C and D are characterized by deformation-dominated flow, and triplet B by shear (Figures 7 and 8). During *e2*, triplet A is governed by deformation (S and N), triplet B by divergence, triplet C by shear (Figures 7 and 8, and shear-to-divergence values ~90), and triplet D by divergence. During *e4*, triplet B is governed by divergence, while during *e6*, triplet B is governed by deformation (N; Figures 7 and 8), and triplets C and D by divergence. During *e7*, triplet B is governed by divergence, as are triplets B to D to a lesser extent during *e8*.